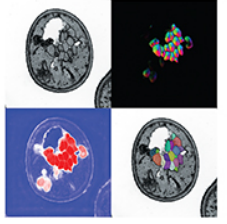


Autophagy





ISSN: (Print) (Online) Journal homepage: www.tandfonline.com/journals/kaup20

Myotubularin 2 interacts with SEC23A and negatively regulates autophagy at ER exit sites in Arabidopsis

Xinjing Li, Jing Zheng, Jing Su, Lin Wang, Lin Luan, Taotao Wang, Fang Bai, Qing Zhong & Qingqiu Gong

To cite this article: Xinjing Li, Jing Zheng, Jing Su, Lin Wang, Lin Luan, Taotao Wang, Fang Bai, Qing Zhong & Qingqiu Gong (08 Sep 2024): Myotubularin 2 interacts with SEC23A and negatively regulates autophagy at ER exit sites in Arabidopsis, Autophagy, DOI: 10.1080/15548627.2024.2394302

To link to this article: https://doi.org/10.1080/15548627.2024.2394302

+	View supplementary material 🗗
	Published online: 08 Sep 2024.
	Submit your article to this journal $oldsymbol{\mathcal{C}}$
ılıl	Article views: 196
a a	View related articles 🗹
CrossMark	View Crossmark data 🗗



RESEARCH PAPER



Myotubularin 2 interacts with SEC23A and negatively regulates autophagy at ER exit sites in Arabidopsis

Xinjing Li^a, Jing Zheng^b, Jing Su^b, Lin Wang^c, Lin Luan^b, Taotao Wang^a, Fang Bai^c, Qing Zhong^d, and Qinggiu Gong 🕞

aState Key Laboratory of Microbial Metabolism & Joint International Research Laboratory of Metabolic and Developmental Sciences, School of Life Sciences and Biotechnology, Shanghai Jiao Tong University, Shanghai, P. R. China; Department of Plant Biology and Ecology, College of Life Sciences, Nankai University, Tianjin, P. R. China; 'Shanghai Institute for Advanced Immunochemical Studies, School of Life Science and Technology, ShanghaiTech University, Shanghai, P. R. China; "Key Laboratory of Cell Differentiation and Apoptosis of Chinese Ministry of Education, Department of Pathophysiology, Shanghai Jiao Tong University School of Medicine, Shanghai, P. R. China

ABSTRACT

Starvation- or stress-induced phosphatidylinositol 3-phosphate (PtdIns3P/PI3P) production at the endoplasmic reticulum (ER) subdomains organizes phagophore assembly and autophagosome formation. Coat protein complex II (COPII) vesicles budding from ER exit site (ERES) also contribute to autophagosome formation. Whether any PtdIns3P phosphatase functions at ERES to inhibit macroautophagy/autophagy is unknown. Here we report Myotubularin 2 (MTM2) of Arabidopsis as a PtdIns3P phosphatase that localizes to ERES and negatively regulates autophagy. MTM2 binds PtdIns3P with its PH-GRAM domain in vitro and acts toward PtdIns3P in vivo. Transiently expressed MTM2 colocalizes with ATG14b, a subunit of the phosphatidylinositol 3-kinase (PtdIns3K) complex, and overexpression of MTM2 blocks autophagic flux and causes over-accumulation of ATG18a, ATG5, and ATG8a. The mtm2 mutant has higher levels of autophagy and is more tolerant to starvation, whereas MTM2 overexpression leads to reduced autophagy and sensitivity to starvation. The phenotypes of mtm2 are suppressed by ATG2 mutation, suggesting that MTM2 acts upstream of ATG2. Importantly, MTM2 does not affect the endosomal functions of PtdIns3P. Instead, MTM2 specifically colocalizes with COPII coat proteins and is cradled by the ERES-defining protein SEC16. MTM2 interacts with SEC23A with its phosphatase domain and inhibits COPII-mediated protein secretion. Finally, a role for MTM2 in salt stress response is uncovered. mtm2 resembles the halophyte Thellungiella salsuginea in its efficient vacuolar compartmentation of Na⁺, maintenance of chloroplast integrity, and timely regulation of autophagy-related genes. Our findings reveal a balance between PtdIns3P synthesis and turnover in autophagosome formation, and provide a new link between autophagy and COPII function.

Abbreviations: ATG: autophagy related; BFA: brefeldin A; BiFC: bimolecular fluorescence complementation; CHX: cycloheximide; ConA: concanamycin A; COPII: coat protein complex II; ER: endoplasmic reticulum; ERES: ER exit site; MS: Murashige and Skoog; MTM: myotubularin; MVB: multivesicular body; PAS: phagophore assembly site; PI: phosphoinositide; TEM: transmission electron microscopy; WT: wild-type.

ARTICLE HISTORY

Received 17 April 2024 Revised 11 August 2024 Accepted 15 August 2024

Autophagy; COPII; ER exit site; myotubularin; PtdIns3P; salt stress

Introduction

Macroautophagy/autophagy is a cytoplasmic degradative pathway that maintains cellular homeostasis and stress adaptation [1,2]. It is a unique membrane trafficking process, in which the biogenesis of a double-membrane vesicle, termed autophagosome, takes the center stage. It begins with the emergence of a phagophore assembly site (PAS) close to the ER, followed by de novo formation of a membrane sac termed phagophore, on phosphatidylinositol-3-phosphate (PtdIns3P)-enriched ER subdomains (omegasomes). Then the phagophore expands and encloses cargoes to form a sealed double membrane autophagosome, which fuses with the vacuole/lysosome to release the cargoes and the enwrapping inner membrane, collectively called the autophagic body, into the vacuole/lysosome for degradation and recycling [3]. Autophagosome biogenesis is catalyzed by a conserved set of core machinery proteins categorized into six functional groups: (i) the Atg1/ULK1 complex; (ii), the class III phosphatidylinositol 3-kinase (PtdIns3K) complex I, or the autophagy-specific complex; (iii) the Atg2-Atg18/WIPI complex; (iv) Atg9-containing vesicles; (v) the Atg12 conjugation system; and (vi) the Atg8/LC3 conjugation system [3,4].

Several membrane sources are known to fuel phagophore formation. The Atg9-containing vesicles either seed the nascent phagophore or transiently deliver lipids and proteins for phagophore expansion [5-7]. Coat protein complex II (COPII)-coated vesicles generated at ERES also provide membranes for phagophore formation [8,9]. The COPII machinery controls ER-to-Golgi transport, and plants have an expanded COPII repertoire [10,11]. Specifically, the Arabidopsis SAR1D-positive COPII vesicles contribute to autophagosome formation [12].

The membrane identity of phagophore and autophagosome is characterized by PtdIns3P [13], which is essential for autophagy [14]. Produced at the ER subdomains by the PtdIns3K complex I, PtdIns3P defines phagophore and autophagosome by recruiting components of all downstream functional groups. PtdIns3P recruits Atg18/WIPI2 to the phagophore [15,16]. Atg18 interacts with Atg2 and tethers phagophore to the ER to facilitate Atg2-mediated phospholipid transport from the ER to the expanding phagophore [17–19]. Atg9 interacts with Atg2-Atg18/WIPI and its scramblase activity is required for phagophore expansion [20,21]. The two conjugation systems are recruited to PtdIns3P-positive membranes via Atg16/ATG16L1, which either binds PtdIns3P-binding WIPI2/Atg21 [22,23], or directly binds PtdIns3P [24].

Apart from phagophore and autophagosome, PtdIns3P also defines endosomes [13,25]. By recruiting effector proteins containing PtdIns3P-binding domains or motifs, PtdIns3P orchestrates endosomal tubulation, multivesicular body (MVB) formation and closure, and fusion of MVB and autophagosome to the vacuole/lysosome [3,13]. To concurrently and specifically carry out these functions, the levels and localization of PtdIns3P must be tightly regulated. Such regulation is achieved by spatiotemporal expression and antagonizing activities of PtdIns3K and the phosphoinositide 3-phosphatases including myotubularins (MTMs) [13]. The catalytic subunit of PIK3C3/VPS34, is encoded by a single gene in all eukaryotes. Knockout of PIK3C3/VPS34 leads to lethality in multi-cellular organisms, including mouse and Arabidopsis [26,27]. PIK3C3/VPS34 inhibitors block both endosomal functions and autophagy [3,13]. The numbers of MTMs vary in yeasts, animals, and plants [28]. The budding yeast (Saccharomyces cerevisiae) encodes only one MTM, Ymr1 [29]. By turning over PtdIns3P at the cytoplasmic side of the mature autophagosome, Ymr1 promotes release of Atg proteins from autophagosome to trigger autophagosome-vacuole fusion [30]. The human genome encodes 16 MTM family members (MTM1, MTMR1-MTMR12, SBF2/MTMR13, MTMR14 and FAN1/MTMR15), 9 catalytically active and 7 inactive. Mutations in MTMs lead to X-linked centronuclear myopathy that results in lethality, myotubular myopathy, or diseases neurodegenerative Charcot-Marie-Tooth [13]. Inactive MTMs, such as MTMR5 and MTMR9, can recruit active MTMs, such as MTMR2 and MTMR6/8, via their C-terminal coiled-coil domain to determine the localization and activity of active MTMs [31,32]. MTM/MTMRs play diverse roles in autophagy. MTMR14/Jumpy, MTMR3, MTMR6 negatively regulate autophagy in the early steps [33,34]. MTMR5 acts with MTMR2 to inhibit autophagy initiation and autophagosome maturation specifically in neurons [35]. Conversely, Drosophila MTMR6 and its mammalian homolog MTMR8 have a positive role in maintaining autophagic flux, and depletion of MTMR6 led to autolysosome accumulation [36]. Apart from its critical function in PtdIns3P-to-PtdIns4P conversion that enables endosomal exocytosis [37], MTM1 is also required for autophagy; Mtm1deficient mice had a reduced autophagic flux and accumulated damaged mitochondria in the muscle [38]. Despite the many reports on animal MTMs that regulate autophagy and

their functional categorization in multiple steps of autophagy, no direct connection between MTMs and ERES has been made.

The Arabidopsis genome encodes two MTMs, MTM1 and MTM2 [39]. Both have PI-3-phosphatase activity *in vitro* [39], however whether and how they may regulate PtdIns3P-mediated trafficking events is unknown. We investigated the function of MTM2 and found out that it specifically antagonizes PtdIns3P-mediated autophagosome formation. We also showed that MTM2 localizes to ERES, where it binds the inner coat component SEC23A with its phosphatase domain and inhibits COPII vesicle formation and secretion of cargo proteins from ERES. MTM2 acts as a powerful switch for basal level, induced, and selective autophagy, and knockout of *MTM2* confers salt stress tolerance to Arabidopsis resembling the behavior of its salt-tolerant relative *Thellungiella salsuginea*.

Results

MTM2 acts towards PtdIns3P and negatively regulates autophagy

MTM2 has been reported to have phosphatase activity toward PtdIns(3,5)P2 and PtdIns3P in vitro [39]. Nevertheless, its phospholipid binding property remains unknown. The domain structure of MTM2 is similar to the catalytically active mammalian MTMs, with an N-terminal PH-GRAM domain, a dual-specificity protein phosphatase (PTP) domain, and a C-terminal coiled-coil domain (CCD) (Figure 1(A)). The PH-GRAM domain is an evolutionarily-conserved Phoxhomology (PH)-like domain that binds to a variety of phosphoinositides [40,41]. We firstly performed Protein Lipid Overlay (PLO) assay with PH-GRAM plus PTP domain of MTM2 (residues 45-491), or PH-GRAM alone (residues 45-161) on lipid strips. The C-terminal coiled-coil domain was not included due to insolubility of a full-length MTM2. Like mammalian MTMs, a truncated MTM2 (aa 45-491) bound to most phosphoinositide (PI) varieties, whereas PH-GRAM (residues 45-161) had higher affinities toward PtdIns3P, PtdIns4P, PtdIns5P and a lower affinity to PtdIns(3,5)P₂ (Figure 1(B)). We further validated the direct binding to PtdIns3P of MTM2 PH-GRAM with liposome co-flotation assay. The PH-GRAM domain of MTM2 could be reconstituted on the liposomes containing 6% PtdIns3P, and thus was found enriched on the top fraction of density gradient after centrifugation. In the negative control condition, in which no PtdIns3P is present at the liposomes, the PH-GRAM domain of MTM2 only remained in lower fractions (Figure 1(C, D)).

The *in vivo* activity of MTM2 toward PtdIns3P or PtdIns(3,5)P₂ was examined by transiently expressing MTM2 with either 2×FYVE, the PtdIns3P probe, or 2×ML1N, the PtdIns(3,5)P₂ probe, in *N. benthamiana* leaf epidermal cells [42,43]. When expressed alone, mRFP-2×FYVE can be found in the cytoplasm and on punctate structures (endosomes or autophagosomes) as reported [44] (Figure 1(E)). MTM2 greatly reduced the 2×FYVE signals, with cytoplasmic signals disappeared and remaining signals accumulated on enlarged vesicles or aggregates (Figure 1E, G),

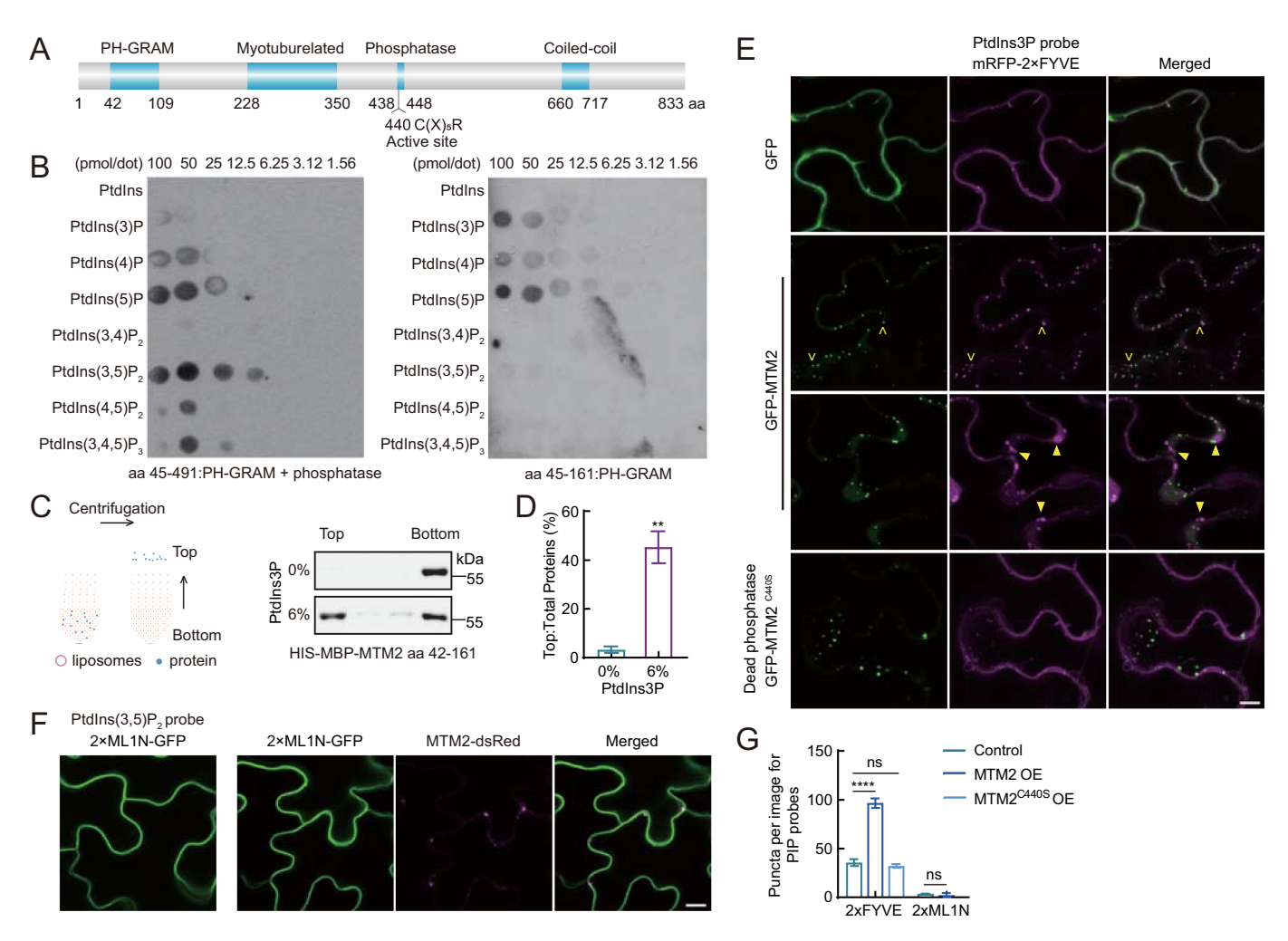


Figure 1. Myotubularin 2 of Arabidopsis binds and acts on PtdIns3P (A) Domain composition of MTM2. MTM2 (aa 1−833) contains an N-terminal PH-GRAM domain (aa 42−109), a myotubularin phosphatase domain (aa 228-448) including active site C440(X)₅R motif, and a C-terminal coiled-coil domain (CCD) (aa 660-717). (B) Protein lipid overlay assay of truncated MTM2 and its PH-GRAM domain. gst-tagged MTM2 without CCD, corresponding to aa 45-491, binds multiple phosphoinositides. gst-tagged PH-GRAM domain of MTM2 (aa 45-161) binds PtdIns3P, PtdIns4P, and PtdIns5P with higher affinities, and PtdIns(3,5)P₂ with a low affinity. Amounts of lipids on the strips are as indicated. Three repeats were done with similar results. (C) Liposome co-floatation assay of MTM2 PH-GRAM domain. When a mixture of liposomes and HIS-MBP-tagged PH-GRAM domain (aa 42-161) of MTM2, was loaded onto a histodenz gradient, MTM2 PH-GRAM was reconstituted on the liposomes containing 6% PtdIns3P and floated to the top fraction of gradient after centrifugation. The top, upper middle, lower middle, and bottom fractions were analyzed with immunoblotting using an anti-his antibody. MTM2 PH-GRAM was enriched in the top fraction only in the presence of 6% PtdIns3P. Liposomes generated without PtdIns3P was used as a blank control. Three repeats were done with consistent results. (D) Quantification of western blots in (C). (E) Colocalization of 2×FYVE (a PtdIns3P probe) with MTM2 (small arrows) and the phosphatase-dead MTM2^{C440S} in N. benthamiana leaf epidermal cells. Overexpression of MTM2 reduces the levels of 2×FYVE, and diminishes its cytoplasmic localization. Remaining 2×FYVE puncta on endosomes and enlarged vesicles or aggregates (large arrowheads) are typical for PtdIns3K inhibition. Expression of the phosphatase-dead MTM2^{C440S} does not affect the subcellular localization of 2×FYVE. GFP served as an expression control. (F) Co-expression of MTM2 and 2×ML1N, a PtdIns(3,5)P₂ probe. Expression of MTM2 does not affect 0×ML1N. (G) Quantification of the nu

****, p<0.0001; **, p<0.01; ns, no significant difference (student's t-test and Tukey's multiple comparisons test). Error bars denote SEM. Bar: 10µm in (E) and (F).

which are typical for PtdIns3P deficiency [45]. In contrast, expression of the phosphatase-dead MTM2^{C440S} did not affect 2×FYVE subcellular distribution (Figure 1E). We also found out that ectopic expression of MTM2 have no effect on 2×ML1N distribution (Figure 1F, G). These findings validated an *in vivo* PI-3-phosphatase activity of MTM2.

PtdIns3P regulates both autophagosome biogenesis and endo-lysosomal trafficking. To see which PtdIns3P-mediated pathway MTM2 May participate in, we obtained a T-DNA insertion mutant, mtm2 ($Salk_147282$) (Figure S1A, F), which had been described previously [39], and characterized its growth and development phenotypes. The mtm2 mutant grew faster than the wild-type (WT) in the soil, produced more rosette leaves, and reached a larger rosette size and

a taller height (Figure S1B-E). These phenotypes were similar to those observed in autophagy-enhancing transgenic plants [46,47]. We also generated complementation lines of *mtm2*, and they were comparable to the WT in all growth parameters measured (Figure S1B-G). Plants that overexpressing *MTM2* also looked like the WT under normal growth conditions (Figure S1B-G).

To see if *mtm2* may indeed have a higher level of autophagy, we generated transgenic lines carrying the autophagy marker *ProUBQ10:GFP-ATG8a* (*GFP-ATG8a*) in the WT and *mtm2* background by crossing, and analyzed the autophagic flux in several ways [48,49]. Previous studies including ours showed that salt stress can induce autophagy within 30 minutes [49,50], hence we firstly treated *mtm2/GFP-ATG8a*

and WT/GFP-ATG8a with 150 mM NaCl plus concanamycin A (ConA), a V-ATPase inhibitor [51], to preserve autophagic bodies in the vacuole for quantification. The number of ATG8a puncta, representing autophagic bodies, was counted before and after NaCl treatment in the root epidermal cells in the transition zone (Figure 2A, B). Compared to the WT, both basal level and NaCl-induced autophagy were significantly higher in mtm2 (Figure 2A, B). We also compared the level of TOR inhibition-induced autophagy in mtm2 and the WT by treating the seedlings with a TOR inhibitor, AZD8055 [52]. Both the basal level autophagy and TOR inhibition-induced autophagy were higher in mtm2 (Figure 2C, D). In contrast, the complementation line was not different from the WT in basal level or induced autophagy (Figure S1H-I). No autophagic flux was observed in the negative control atg5/GFP-ATG8a (Figure 2A-D, Figure S1J). We further examined the level of selective autophagy receptor NBR1 in mtm2 and the WT, which marks the level of selective autophagy since it is degraded along with autophagy cargoes in the vacuole [53]. At normal growth condition, mtm2 has less NBR1, indicative of induced selective autophagy. TOR inhibition reduced the difference in NBR1 levels between mtm2 and the WT, which is restored by treating the plants with both AZD8055 and E64d, a cysteine protease inhibitor that partially inhibits protein degradation in the vacuole. These results suggested that selective autophagy, represented by NBR1 consumption, is also higher in mtm2 (Figure 2E, F). The fact that MTM2 negatively regulates basal level, salt-induced, starvation-induced, and selective autophagy suggested that it may directly participate in autophagosome formation at an early stage.

MTM2 specifically antagonizes PtdIns3P-mediated autophagosome formation

To explore the function of MTM2 in autophagosome formation, we co-expressed representative core ATG proteins of four functional groups with MTM2 to see if MTM2 overexpression may affect their localization patterns. The ATG1 kinase complex was represented by ATG13a [54], the PtdIns3K complex was represented by ATG14b [55], the ATG2-ATG18 complex was represented by ATG18a [56], and the ATG12 conjugation system was represented by ATG5 [57] (Figure 3A). First of all, MTM2 significantly colocalized with ATG14b (Figure 3A-C), suggesting that MTM2 is localized to the PtdIns3P-production site specific for autophagy, i.e. the phagophore. Neither ATG13a nor ATG14b were affected by MTM2 overexpression (Figure 3A-C), suggesting that ATG1 and PtdIns3K complexes act upstream of MTM2. Conversely, localization of ATG18a and ATG5 are strongly affected; both accumulated on enlarged puncta only when MTM2 is overexpressed, as indicated by Mander's colocalization coefficients (Figure 3A-C). We then examined how GFP-ATG8a localization and autophagic flux

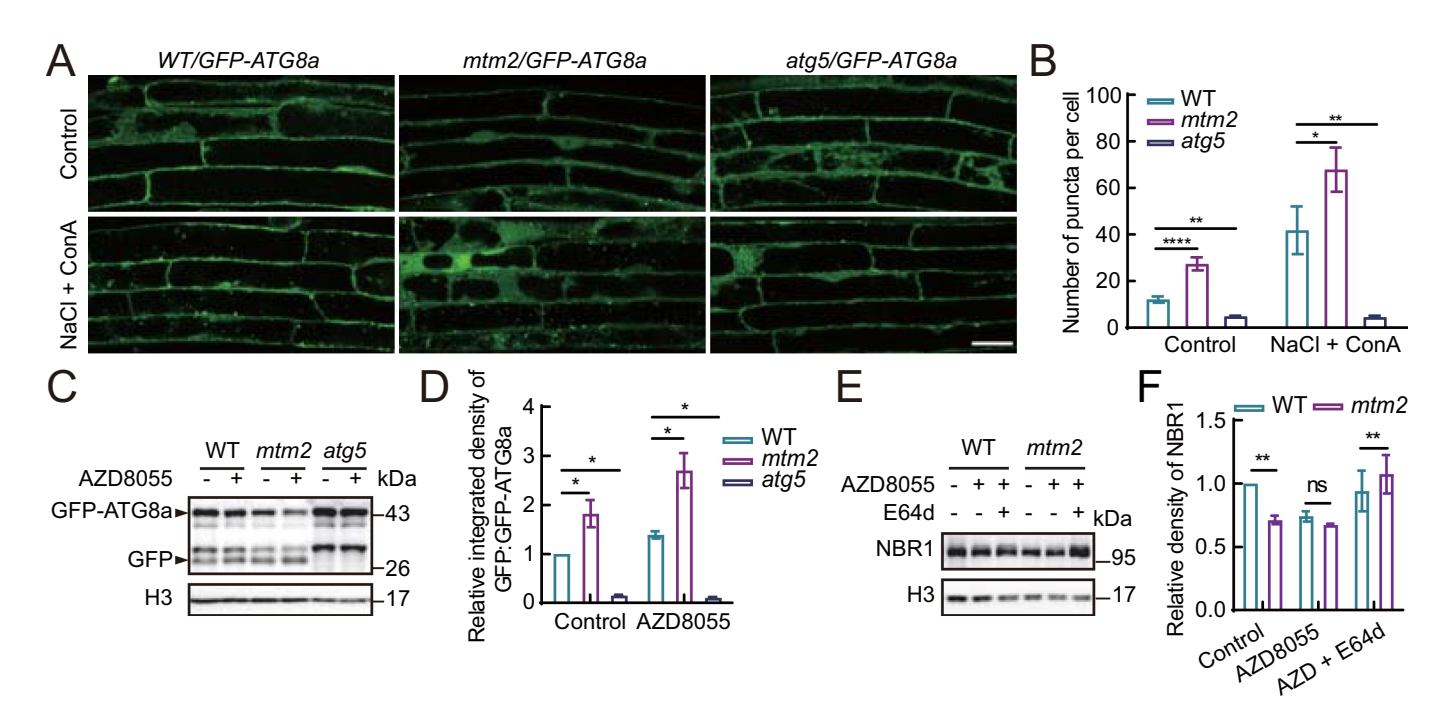


Figure 2. The mtm2 null mutant has higher levels of autophagy (A) confocal images of GFP-ATG8a in root epidermal cells in the transition zone of GFP-ATG8a, mtm2/GFP-ATG8a, and atg5/GFP-ATG8a, with or without 30 min of 150 mM NaCl plus 0.5 μM concanamycin a (ConA) treatment. More GFP-ATG8a puncta were observed in mtm2 before and after salt treatment. atg5 served as a negative control. At least 30 seedlings from five biological replicates were scanned in Z-axis, and one representative image is shown for each condition/genotype. Bar: 25 μm. (B) Quantification of the number of autophagosomes in (A) in the lytic vacuoles of epidermal cells. (C) GFP-ATG8a cleavage assay, indicative of autophagic flux induced by the TOR inhibitor AZD8055, was performed in WT and mtm2. GFP-ATG8a and free GFP were detected with anti-gfp. Free GFP accumulated more in mtm2 than in the WT. Anti-histone H3 (H3) was used as a loading control. (D) statistics of relative density of free GFP-GFP-ATG8a, representing autophagic flux, in (C). (E) Western blot analysis of the selective autophagy receptor/adaptor NBR1, detected with anti-NBR1. WT and mtm2 were treated with or without 1 μM AZD8055 and 100 μM E64d, a cysteine protease inhibitor that antagonizes vacuolar protein degradation. mtm2 has less NBR1 than the WT with or without AZD treatment. (F) Quantification of NBR1 levels in (E).

^{****,} p < 0.0001; **, p < 0.01; *, p < 0.05; ns, no significant difference (Tukey's multiple comparisons test and student's t-test). Error bars denote SEM.

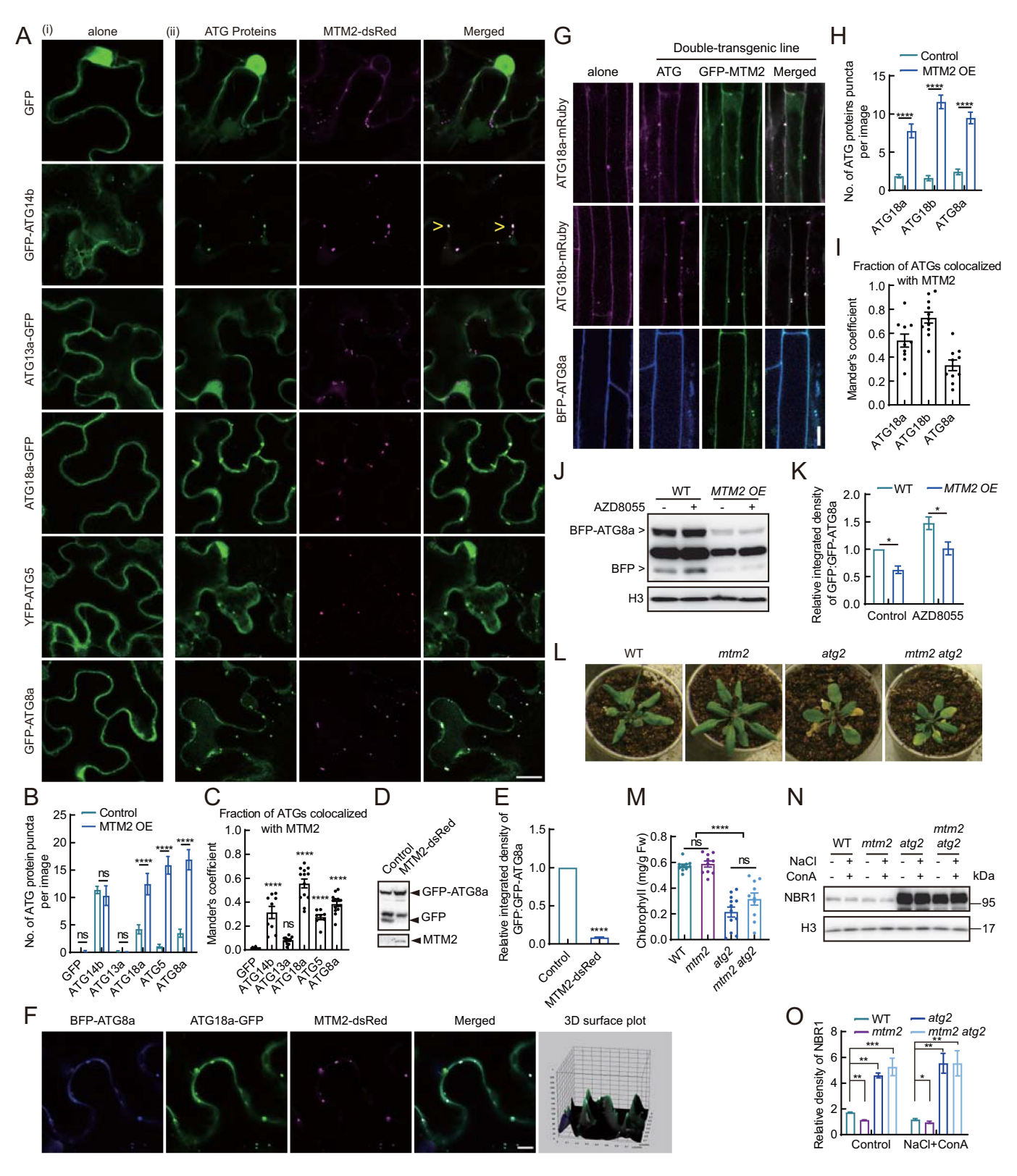


Figure 3. MTM2 negatively regulates PtdIns3P-mediated autophagosome formation and autophagy (A) (i) subcellular localization of GFP- or yfp-tagged ATG core machinery proteins alone in transiently-transformed *N. benthamiana* leaf epidermal cells; (ii) subcellular localization of same ATG proteins co-expressed with MTM2-dsRed. Overexpression of MTM2 does not change the distribution of GFP, ATG13a, and ATG14b, however induces aggregation of ATG18a, ATG5, and ATG8a. Note that MTM2 and ATG14b colocalize (arrowheads). (B) quantification of ATG protein puncta in (A). (C) Quantification of colocalization of the ATG proteins and MTM2 in (A) with the Mander's coefficient. (D) immunoblot of GFP-ATG8a alone or co-expressed with MTM2-dsRed in (A). Overexpression of MTM2 blocked GFP cleavage, indicative of inhibited autophagic flux. Arrowheads denote the right bands of proteins. Anti-MTM2 only detected overexpression of MTM2. (E) Quantification of intensity of GFP:GFP-ATG8a in (C), which Indicates autophagic flux. (F) Both ATG8a and ATG18a accumulated at where MTM2 puncta reside when all three proteins are co-expressed in *N. benthamiana*. 3D surface plot illustrates the colocalization of all three proteins. (G) in Arabidopsis double-transgenic lines, GFP-MTM2 colocalized with ATG18a-mRuby, ATG18b-mRuby, and BFP-ATG8a at punctate structures. Root epidermal cells in the elongation zone are shown. (H, I) Quantification of ATG protein puncta and statistics of their colocalization with MTM2. The Mander's colocalization coefficient was calculated for each ATG-MTM2 pair. (J) Western blot analysis of autophagic flux, indicated by BFP-ATG8a cleavage assay, in WT and *proUBQ10:GFP-MTM2* with or without AZD8055. Overexpression of MTM2 strongly inhibited BFP-ATG8a degradation with or without TOR inhibition, indicative of blocked basal level and starvation-induced autophagy. anti-histone H3 (H3) was used

can be affected by MTM2 overexpression (Figure 3A-C, Figure S2A-C). Overexpression of MTM2 did increase the size of GFP-ATG8a puncta, whereas overexpression of MTM2^{C440S}, the phosphatase-dead MTM2, did not change the size of GFP-ATG8a puncta, although they both increased the number of GFP-ATG8a puncta (Figure S2A-C). This observation is similar to a report on *Drosophila* Mtmr6, in which defective autophagy and increased and enlarged Atg8a

blocked by MTM2 overexpression (Figure 3D, E). We also validated that ATG8a, ATG18a, and MTM2 colocalized to enlarged puncta when MTM2 is overexpressed (Figure 3F). We further generated Arabidopsis double-transgenic lines carrying both *GFP-MTM2* and *ATG18a-mRuby*, *ATG18b-DED ATG18* Constitution of the state of th

puncta were observed in dMtmr6-knockdown enterocytes

[36]. Meanwhile, the autophagic flux is nearly completely

carrying both GFP-MTM2 and ATG18a-mRuby, ATG18bmRuby, or BFP-ATG8a. Consistent with the observations in N. benthamiana, changes in subcellular distribution were observed for ATG18a, ATG18b, and ATG8a in the doubletransgenic lines. ATG18a and ATG18b accumulated on cytoplasmic puncta when MTM2 is overexpressed, and they colocalized with MTM2 as indicated by Mander's colocalization coefficients (Figure 3G-I). The number of ATG8a puncta also increased, and ATG8a partially colocalized with MTM2 in the cytoplasm (Figure 3G-I). The autophagic flux, represented by BFP-ATG8a cleavage, was blocked in GFP-MTM2 and BFP-ATG8a double-transgenic plants (Figure 3J, K). For some unknown reason, MTM2 overexpression led to a reduction in the protein level of full length BFP-ATG8a (Figure 3J). The observations in N. benthamiana and Arabidopsis suggested that the autophagy functional groups downstream of the PtdIns3K complex are affected by a reduction of PtdIns3P and accumulated.

The yeast and animal ATG2 transports phospholipids from the ER to the expanding phagophore with the help of PtdIns3P effector ATG18/WIPI [18]. Since ATG18 has eight isoforms, whereas ATG2 is a single gene in Arabidopsis, we carried out genetic analyses on ATG2 and MTM2 to see if atg2 can suppress the autophagy-enhancing phenotypes of mtm2. Like atg2, mtm2 atg2 displayed typical autophagy-deficient phenotypes: It had a smaller size than the WT and senesced earlier (Figure 3L, M), was more sensitive to nitrogen- (-N) and carbon- (-C) starvation in liquid culture (Figure S1K-L, Figure S2D-G). Plants overexpressing MTM2 also senesced earlier than the WT under nitrogen starvation, which is typical for autophagy-deficient mutants including atg2 (Figure S2D, F). Immunoblotting of NBR1 following NaCl treatment confirmed that selective autophagy is also abolished in mtm2 atg2 like in atg2 (Figure 3N, O). We concluded that atg2 is epistatic to mtm2.

Since PtdIns3P is a key regulator of endo-lysosomal trafficking routes, such as endocytosis, MVB formation, and MVB and autophagosome fusion with the vacuole, a PI 3-phosphatase that regulate endosomal activities may also control the last step of autophagy, i.e. autophagosomevacuole fusion, like in budding yeast [30]. We precluded this possibility with several lines of evidence. Firstly, no colocalization between MTM2 and markers of the Golgi (Golgi-gk), trans-Golgi network (TGN) (SCAMP1-GFP), the early and late endosomes (ARA6-GFP and GFP-RHA1), or the tonoplast (Vacuole-gk), was observed (Figure S3A and B). Secondly, we evaluated the impact of MTM2 deletion on the endo-lysosomal pathway and saw no difference between mtm2 and the WT (Figure S4). Sorting of seed storage proteins, 2S albumin and 12S globulin, into the protein storage vacuole (PSV) [58], was normal in mtm2 (Figure S4A), indicative of normal vacuolar protein sorting (VPS). The rates of endocytosis, indicated by the internalization of the styryl dye FM 4-64, were comparable in mtm2 and the WT (Figure S4B) and C). Furthermore, the rates of brefeldin A (BFA) compartment formation and BFA washout-induced polar exocytosis of the auxin efflux carrier PIN2 were comparable in mtm2 and the WT (Figure S4D-F), indicative of normal activities of early and recycling endosomes [59]. Finally, dark-induced vacuolar transport of PIN2-GFP was normal in mtm2 (Figure S4G and H), suggesting that MVB formation and fusion to the vacuole is unaffected by MTM2 deficiency. We concluded that MTM2 is a specific negative regulator of autophagy that functions at an early stage.

MTM2 localizes to ER exit sites (ERES)

We then asked how MTM2 can antagonize autophagy at an early stage. First, we co-expressed MTM2 with an ER membrane marker DERLIN1 and found out that MTM2 puncta are transiently associated with, instead of retained in the ER (Figure 4A). Apart from Golgi [60], ERES, or transitional ER (tER), are known to have such behavior [61-64]. ERES is the site for COPII vesicle budding, and certain COPII vesicles serve as membrane source for autophagosome formation in Arabidopsis [12,65]. Nevertheless, whether and how a PI 3-phosphatase can function at ERES in any eukaryotes is unknown. To see if MTM2 can localize to ERES, we coexpressed MTM2 with an ER marker, SAR1 NT. SAR1 NT corresponds to the N-terminal amphipathic helix (AH) of SAR1 [66]. Activated SAR1 exposes this helix to insert into the ER before it induces COPII vesicle assembly at ERES [66]. Indeed, MTM2 colocalized with SAR1 NT on punctate structures that are likely ERES (Figure 4A).

To dissect the relationship between MTM2 and ERES, we employed TurboID-based proximity labeling coupled with mass spectrometry/PL-MS [12,67,68], and captured MTM2-interacting and/or proximal proteins in transiently

^{****,} p < 0.0001; ***, p < 0.001; **, p < 0.01; *, p < 0.05; ns, no significant difference (Student's t-test and Tukey's multiple comparisons test). Error bars denote SEM. Bar: 10 μ m in (A), (F) and (G). Diameter of pot: 6.5 cm in (L).

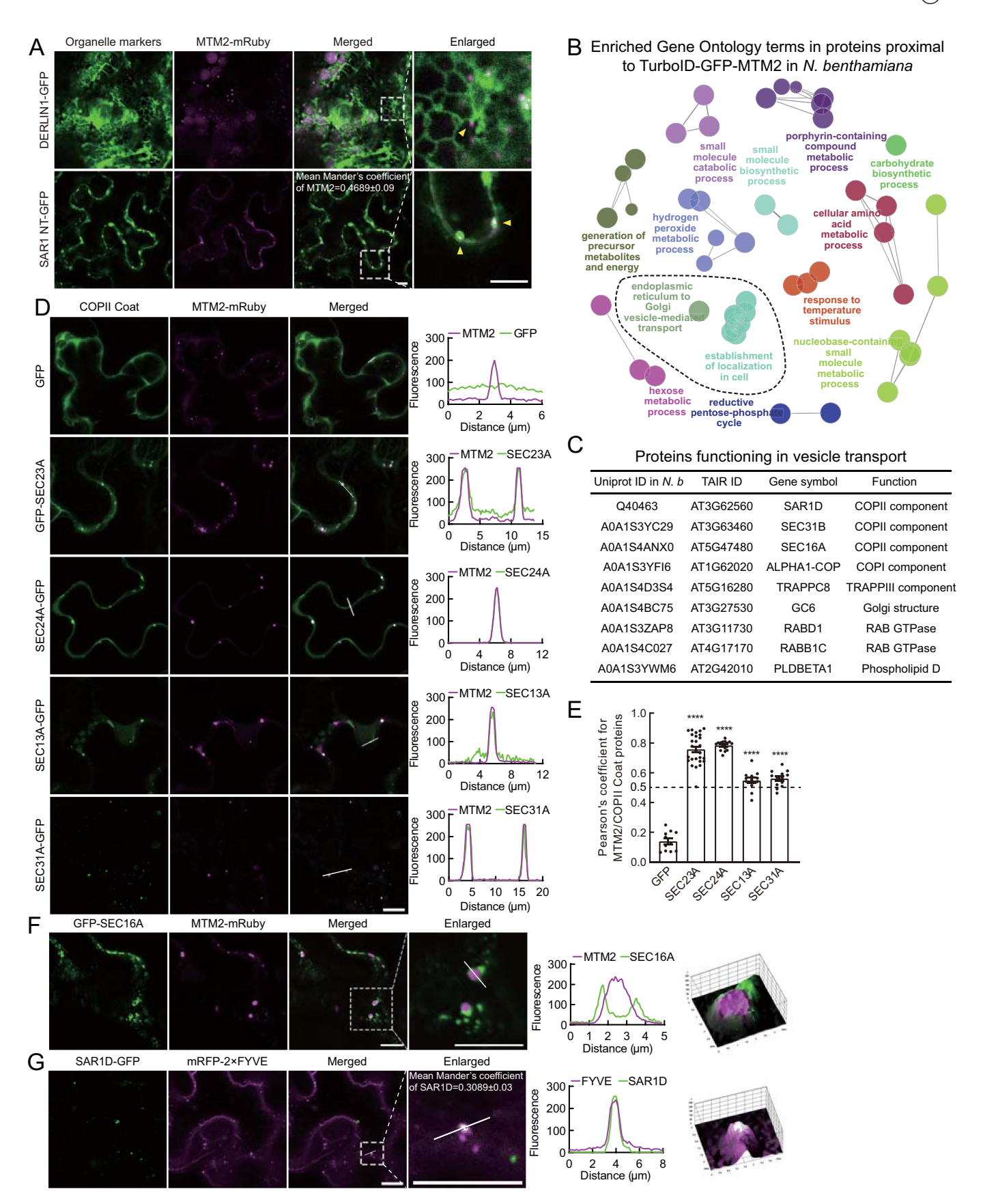


Figure 4. MTM2 localizes to ER exit sites (ERES) with COPII coat components and SEC16A, the ERES marker (A) Co-expression of MTM2 and ER membrane marker DERLIN1 and the ER and ERES marker SAR1 N-terminal helix (SAR1 NT) in *N. benthamiana*. MTM2 is localized to the rim of ER network (arrowhead) (upper panel). MTM2 colocalized with SAR1 NT on punctate structures (arrowheads) (lower panel). The Mander's colocalization coefficient is 0.4689 for MTM2 colocalized with SAR1 NT, SEM = 0.09. (B) TurboID-based proximity labelling coupled with mass spectrometry identified 350 proteins as specifically proximal to TurboID-GFP-MTM2 in *N. benthamiana*. Among them, ER to golgi vesicle-mediated transport and establishment of localization in cell were the only two enriched gene ontology (GO) terms in the cellular component category. (C) Selected proteins in the dotted circle in (B); both uniprot ID for the *N. benthamiana* proteins identified and their closest

transformed N. benthamiana. Three hundred and fifty proteins were specifically associated with MTM2 (Table S1). Among them, Gene Ontology (GO) terms ER-to-Golgi vesicle-mediated transport and establishment of localization in cell were the only two enriched GO cellular component categories (Figure 4B). Notably, N. benthamiana homologs of Arabidopsis COPII components SAR1D, SEC31B, and SEC16A, were identified as proximal to MTM2 (Figure 4C). Indeed, MTM2 colocalized with components of both the COPII inner coat complex SEC23/SEC24 and the outer coat complex SEC13/SEC31 (Figure 4D-E, Movie S1-4.). Strikingly, all MTM2 puncta were cradled by SEC16A, the scaffold protein for COPII coat assembly and marker for ERES [69], which formed cup-shaped structures that are known to be ERES (Figure 4F, Movie S5) [69]. Clearly, MTM2 is localized to ERES. The presence of PtdIns3P at ERES was also confirmed by colocalization of the PtdIns3P probe 2×FYVE and SAR1D, the SAR1 GTPase that specifically promotes autophagy in Arabidopsis (Figure 4G) [12].

MTM2 interacts with SEC23A to inhibit specific COPII **function**

We further explored the relationship between MTM2 and COPII components since COPII vesicles fuels autophagosome formation. The TurboID results mainly informed us of where MTM2 localize to; thus, to see which COPII component may be an interacting partner for MTM2, we carried out a mini protein-protein interaction screen using bimolecular fluorescence complementation (BiFC) in N. benthaminana. SEC23A, the GTPase activating protein/GAP for SAR1 and inner coat component, was identified as a MTM2-interacting partner (Figure 5A, Figure S5A and B). The interaction between SEC23A and MTM2, revealed by BiFC, takes place at SEC31A-positive structures, likely COPII (Figure 5B). We also generated double-transgenic lines carrying GFP-MTM2 and mRuby-SEC23A, and observed both transient and relatively stable colocalization of MTM2 and SEC23A (Movie S3 and 4). The interaction between MTM2 and SEC23A further explored with coimmunoprecipitation and structural modeling (Figure 5C). Co-immunoprecipitation of protein N. benthamiana leaves expressing GFP-SEC23A and MTM2dsRed confirmed their interaction (Figure 5D). We then mapped the SEC23A binding region on MTM2 using recombinant proteins, and found out that MTM2 interacts with SEC23A with its PTP domain (residues 181-647), but not with the PH-GRAM domain (residues 42-161) (Figure 5E). We also found out that the order region of SEC23A (residues

157-880) is the interacting partner for MTM2 PTP domain (Figure 5E, F, I).

Since crystal structures of mammalian myotubularins MTMR1, MTMR2, MTMR6, and MTMR8 [70,71] and yeast and mammalian COPII coat protein complexes are available [72,73], we built MTM2 and SEC23A structural models on the reported crystal structures, and further determined their binding interface using AlphaFold-Multimer [74], an extension of AlphaFold2 specifically trained to model protein complexes. The binding interface of MTM2 is dominated by residues 264-509, which corresponds to a group of helices within the PTP domain. MTM2 and SEC23A form a tight complement of shape and hydrophobic properties, with the formation of four hydrogen bonds on the binding interface (Figure 5H). This predicted binding interface was verified by an in vitro affinity-isolation assay (Figure 5I). Furthermore, we found out that strong co-evolution exists between the N-terminal disorder region (residues 1-157) of SEC23A and the PTP domain of MTM2 (Figure S5C-D). Interestingly, this disorder region is only found in SEC23A, but not in other SEC23 isoforms. It is likely that both the disorder region and the order region contribute to the interaction (Figure 5D-E). Together, these results validated the interaction between MTM2 and SEC23A in vivo and in vitro.

We also examined the impact of gain and loss of function of MTM2 on protein secretion, a trafficking route initiated by COPII vesicle formation at ERES. RNA sequencing revealed that, in mtm2, genes encoding proteins functioning at the PM for osmotic adjustment or cell wall biosynthesis had higher transcript levels (Figure 6A). Particularly, these included the proline transporter PROT2 [75], the sucrose and biotin transporter Suc5 [76], and the abscisic acid (ABA) transporter ABCG40 [77], which have been identified as cargoes of plant specific, abscisic acid-induced giant COPII vesicles [78]. Consistently, MTM2 overexpression led to the ER retention of PROT2, which appeared to accumulate at ERES (Figure 6B,C). Compared with the WT, mtm2 had a significantly higher level of secreted proteins in the apoplast (Figure 6D,E). We further generated mtm2- and WT-background transgenic lines that carry secGFP, a secreted form of GFP that serves as a marker for protein secretion [79], and compared the GFP intensity in the root. In mtm2, secGFP delivered to the apoplast and vasculature accumulated to a much higher level than in the WT (Figure 6F,G). Together, these data support a role for MTM2 in attenuating COPII function.

Knockout of MTM2 confers salt tolerance to Arabidopsis

Previous studies including ours have demonstrated that autophagy responds Quickly to salt stress, and facilitates salt stress

arabidopsis homologs (TAIR ID) are shown. (D) COPII coat components, including inner coat SEC23/24 and outer coat SEC13/31, were co-expressed with MTM2mRuby in N. benthamiana. MTM2 colocalized with COPII coat proteins SEC23A, SEC24A, SEC13A, and SEC31A. GFP served as a blank control. (E) colocalization of MTM2 and COPII components, as indicated by the Pearson's coefficients calculated from (D). A > 0.5 Pearson's coefficient indicates positive correlation. n > 12 images for each. (F) MTM2 is embedded in the cup-like structure labelled by SEC16A, the scaffold protein for COPII and ERES marker in N. benthamiana. (G) SAR1D, a GTPase responsible for initiating COPII assembly, is co-expressed with 2×FYVE, a PtdIns3P probe in N. benthamiana. Colocalization can be seen for SAR1D and 2×FYVE. The Mander's colocalization coefficient is 0.3089 for SAR1D colocalized with 2×FYVE, SEM = 0.03. Fluorescence intensity profiles were calculated along the white lines indicated in (D), (F), and (G) to show signal distribution of gfp-tagged proteins and MTM2-mRuby or mRFP-2×FYVE. 3D surface plot illustrates the colocalization of protein pairs in (F) and (G). Bar: 10 µm in (A), (D), (F), and (G).

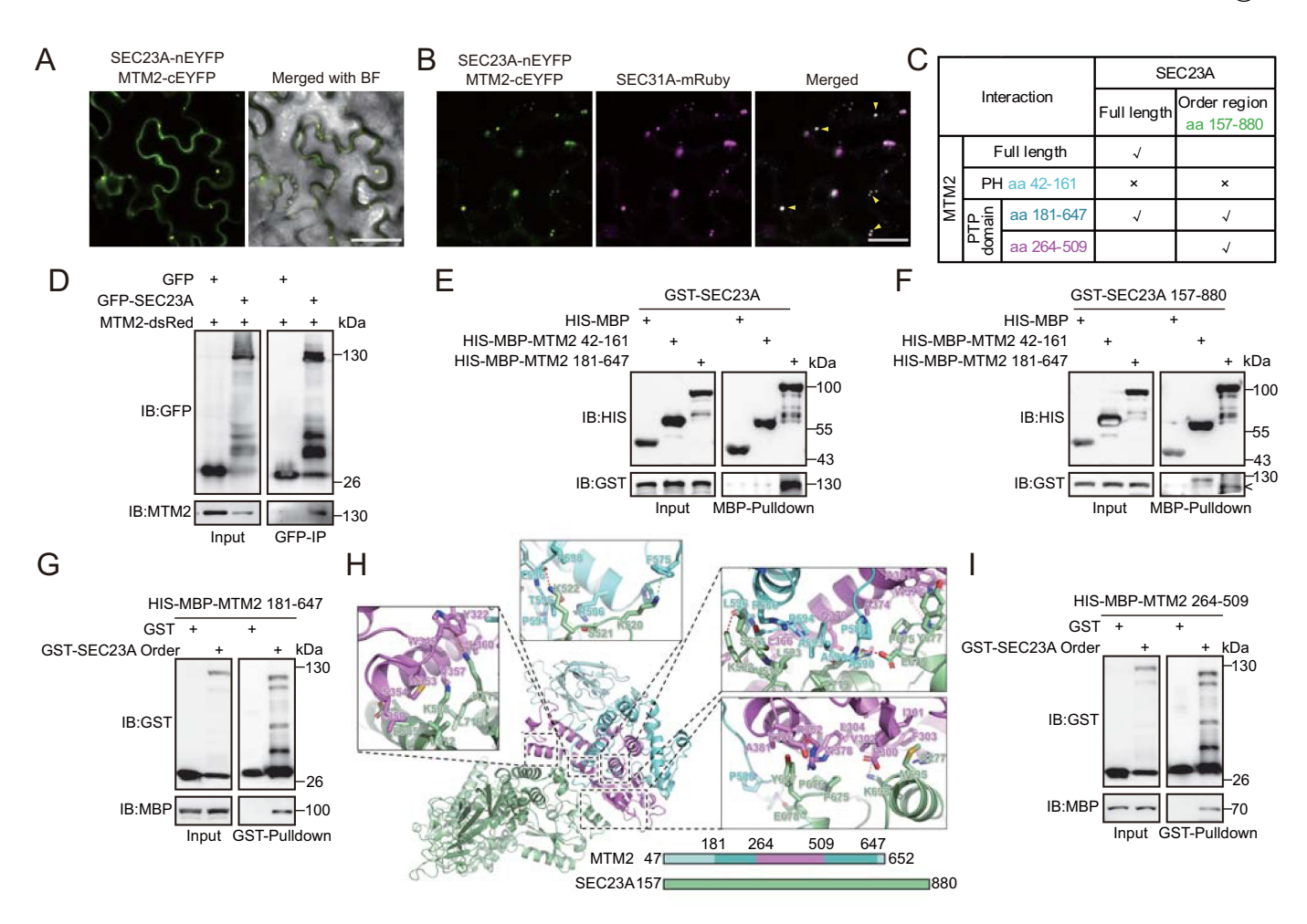


Figure 5. Interaction between MTM2 and SEC23A (A) BiFC assay revealed an interaction between MTM2 and SEC23A in *N. benthamiana*. Both cytoplasmic and punctate signals can be seen. (B) Co-expression of SEC23A-nEYFP, MTM2-cEYFP, and SEC31A-mRuby. MTM2 and SEC23A interacted on SEC31A-positive puncta (marked with arrowheads), i.e. ERES. (C) Summary of the interaction between MTM2 and SEC23A mapped from co-immunoprecipitation assays. (D) Co-immunoprecipitation of GFP-SEC23A with MTM2-dsRed *in planta*. MTM2-dsRed was co-transformed with GFP or GFP-SEC23A in *N. benthamiana* leaves; proteins were immunoprecipitated with GFP-Trap, detected by anti-gfp and anti-MTM2. GFP was used as a negative control. (E, F) MBP affinity-isolation assay between SEC23A, SEC23A aa 157–880, and MTM2 aa 42-161 (PH-GRAM domain), 181-647 (PTP domain). The order region of SEC23A interacts with the MTM2 PTP domain. The co-sonicated protein supernatant was incubated with MBP agarose beads for 2 h, followed by washing and subsequent detection with GST and MBP antibodies, "<"indicates the correct band size. (G) GST affinity-isolation assay between HIS-MBP-MTM2 aa 181-647 (PTP domain) and GST-SEC23A aa 157-880 (order region). (H) MTM2-SEC23A complex structure predicted with AlphaFold-Multimer. MTM2 (aa 47-652) was colored in different colors as indicated and SEC23A (aa 157-880). (H) MTM2-SEC23A complex structure predicted with AlphaFold-Multimer. MTM2 (aa 47-652) was colored in different colors as indicated and SEC23A (aa 157-880) was colored in pale green. The MM/GBSA binding energy of the binding interface is −107.46 kcal/mol. (I) based on the interaction interface calculations, the interaction of HIS-MBP-MTM2 residues 264-509 and GST-SEC23A order region was confirmed by GST pull-down assay. Bar: 50 μm in (A) and 20 μm in (B).

adaptation [49,50,80]. The fact that mtm2 have increased level of autophagy suggested that it may have better salt tolerance. We analyzed the salt-response phenotypes of mtm2 using atg mutants as negative controls. On 150 mM NaCl, true leaves emerged earlier in germinating mtm2 seedlings compared with the WT (Figure 7A-C). In contrast, true leaves of MTM2-overexpressing seedlings emerged later, and the complemented line behaved like the WT (Figure 7A,D). Since autophagy is employed in the clearance of damaged chloroplasts or chloroplast-derived vesicles [81], we also compared the shape and ultrastructure of WT and mtm2 chloroplasts upon NaCl treatments. In salt-treated 11-day-old WT seedlings, chloroplasts became swollen with disorganized thylakoid membranes and accumulated plastoglobuli, implying damages in chloroplast structure and function. In contrast, chloroplasts were normal in size and shape in mtm2 (Figure 7E,F). RNA sequencing of mtm2 and WT revealed that, nuclear- and chloroplast-encoded proteins functioning in chloroplast transcription (RPOA, RPOB, and RPOCs) and translation (RPLs and RPSs), as well as proteins functioning in photosynthesis, all had much higher transcript levels in *mtm2* after 1 h of salt treatment compared with the WT (Figure 7G,H). These results indicated that *mtm2* maintains normal chloroplast function under salt stress.

A typical strategy for salt tolerance is the compartmentalization of Na⁺ into the vacuole [2,49,82,83]. CoroNa Green staining of Na⁺ revealed that, in the primary root, after 6 h of 100 mM NaCl treatment, *mtm2* accumulated more Na⁺ in the vacuoles of the cortex cells (Figure 7I,J). RNA-sequencing analysis showed that, under normal growth condition, *mtm2* already induced the expression of transporters responsible for salt tolerance (Figure 7K), as we have seen on transporters that function in osmotic adjustment (Figure 6A). Transcript levels of these transporters were induced in the WT only after salt treatment, whereas *mtm2* already reduced their expression within 1

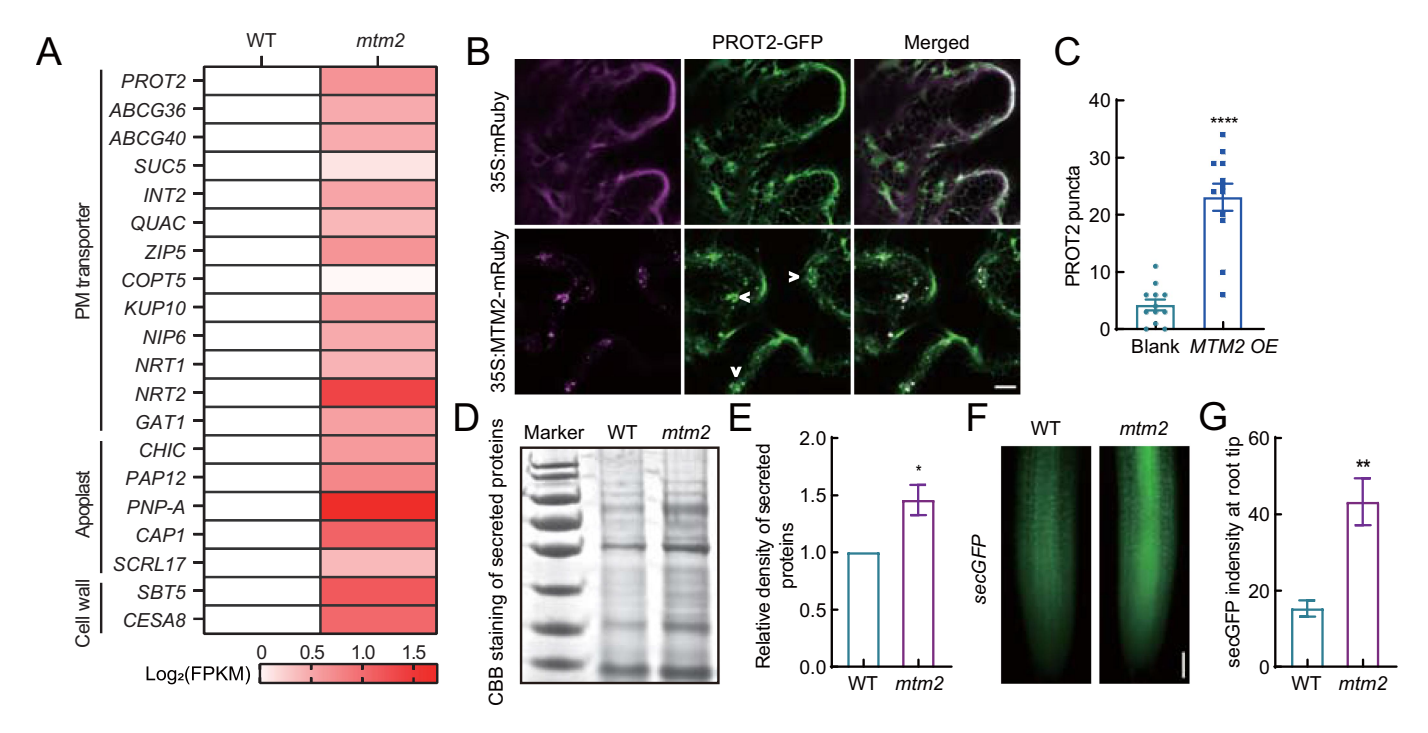


Figure 6. MTM2 negatively regulates copii-mediated protein secretion (A) heat map showing the elevated transcript levels of selected proteins that localize to PM or apoplast in *mtm2*. Each grid represents the log₂ (FPKM) value normalized to that of WT. (B) *Pro355:MTM2-mRuby* and *PROT2-GFP* were co-expressed in *N. benthamiana* leaves. Overexpression of MTM2 resulted in retention of the proline transporter PROT2 in the ER (arrowheads) at where MTM2 reside. *Pro355:mRuby* was used as a negative control. (C) Quantification of the number of PROT2-GFP puncta in (B). (D) Coomassie brilliant blue (CBB) staining of secreted proteins obtained by centrifugation from 4-week-old rosettes of WT and *mtm2*. More secreted proteins accumulated in the apoplast in *mtm2*. Three replicates were done, and a representative gel is shown. (E) Quantification of secreted proteins in (D). (F) Distribution of secGFP in the root tip of WT and *mtm2*. More secGFP is detected in the apoplast and in the vasculature in *mtm2*. At least 10 roots were scanned in each genotype with similar results. (G) Quantification of GFP intensity at root tip in (D). Bar: SEM.

****, p < 0.0001; **, p < 0.01; *, p < 0.05 (student's t-test). Bar: 10 μ m in (B) and 100 μ m in (F).

h. Such behavior is reminiscent of the halophyte *Thellungiella salsuginea*, which had an "anticipation" for stress by keeping the transcript levels of key transporters high at normal growth condition, and can tune down stress response and resume growth timely under moderate salt stress [84].

We further analyzed the transcript levels of key autophagy genes in response to salt in mtm2 and the WT. RNAsequencing showed that, response to salt stress was among the top GO terms preferentially induced in mtm2 treated with NaCl (Figure S6A). Consistent with the fact that basal level autophagy is higher in mtm2, genes encoding autophagy machineries were mostly induced in the WT within 1 h of salt stress, yet only ATG8s were significantly induced in mtm2, and the regulators upstream of PtdIns3P were mostly downregulated in mtm2 at this time point (Figure S6B). Quantitative RT-PCR confirmed that many ATG genes were slightly repressed at 1 h, then induced to peak at 3 or 6 h, then repressed in both WT and mtm2, and that the induction at 3 or 6 h was overall stronger in mtm2 (Figure S6C). The time course of ATG gene induction and repression agrees with previous autophagy flux studies including ours, which showed that autophagy responds quickly to salt stress, and gets repressed after around 6 h [49,50,80]. It is noteworthy that the induction of ATG genes by NaCl at 3h, including ATG8 and ATG18, had also been observed in the salt tolerant relative of Arabidopsis, Thellungiella salsuginea [84].

We finally examined whether and how MTM2 itself can be regulated by salt stress. The transcript level of MTM2 is induced mainly at 3- and 6-h of salt treatment (Figure S7A). GUS staining of ProMTM2:GUS confirmed an induction of MTM2 promoter activity after 6-h of salt treatment in the young leaves and hypocotyls (Figure S7B). Notably, MTM2 protein level was constant during the first hour of salt treatment, and quickly accumulated to high levels upon 3-24 h (Figure S7C and D), coinciding with our previous observation that NaCl-induced autophagic flux is tuned down after an initial boost [49]. By inhibiting protein degradation with the 26S proteasome inhibitor MG132, we found out that MTM2 accumulation under prolonged salt treatment is likely due to more MTM2 protein synthesis (Figure S7E and F). By combining the protein synthesis inhibitor cycloheximide (CHX) and MG132 or ConA treatments, it was revealed that MTM2 degradation was more likely 26S proteasome dependent, rather than autophagy dependent (Figure S7G-I). We concluded that MTM2, a negative regulator of autophagy, is kept at low levels under normal growth condition (hence hard to observe at the control condition), and its synthesis can be induced by prolonged stress, such as 6 h of salt stress, so that the already induced autophagy can be tuned down to save resource and energy. The tight regulation on MTM2 expression and degradation likely help ensure timely modulation of autophagic flux. How MTM2 biosynthesis and degradation is regulated by salt stress awaits future exploration.

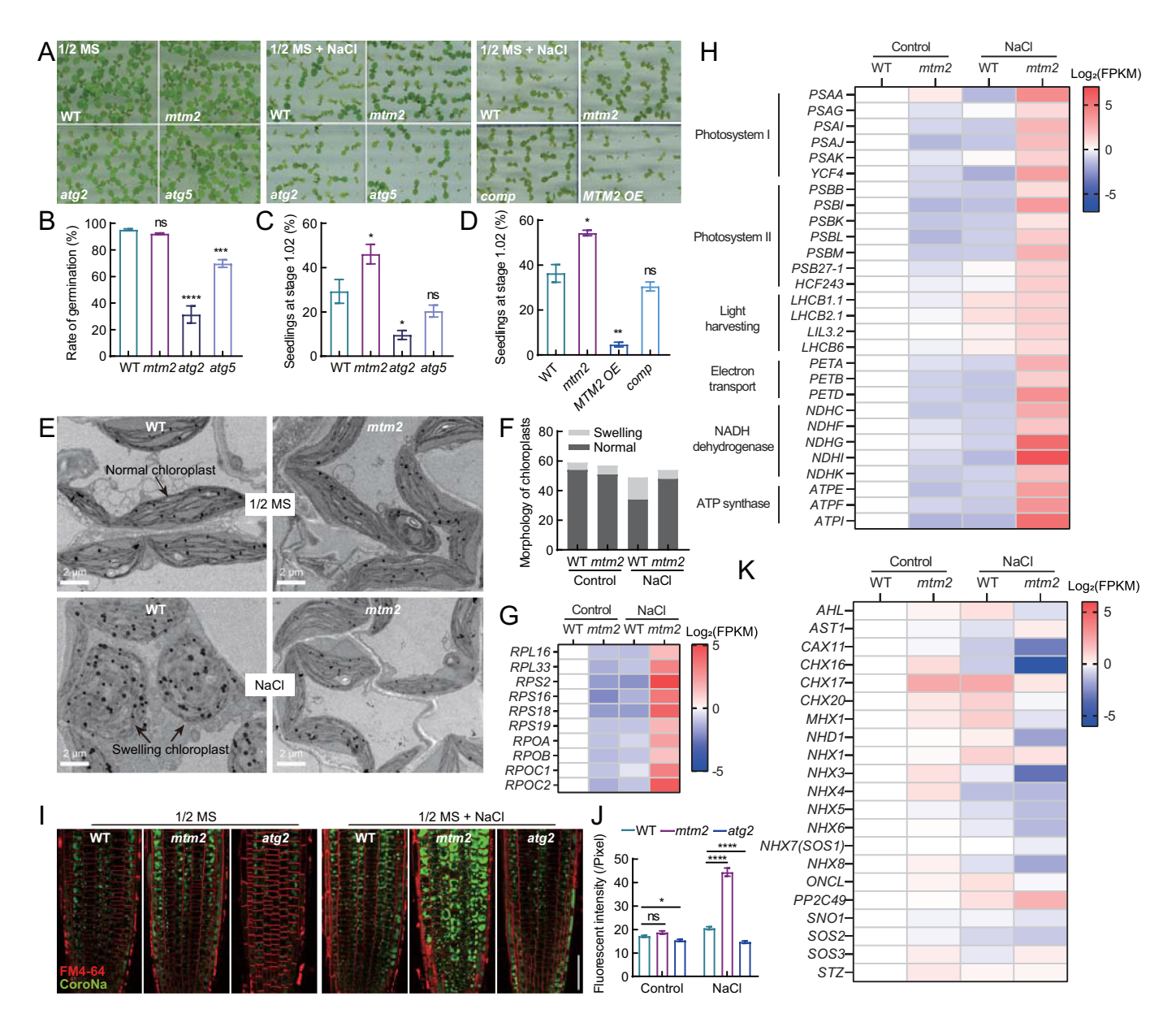


Figure 7. Knockout of MTM2 confers salt tolerance to Arabidopsis (A) Ten-day-old seedlings geminated and grown on 1/2 MS plates with or without 150 mM NaCl. The mtm2 mutant grows better than WT on salt. The complementation line (comp) was similar to WT. The MTM2 overexpression line $(MTM2 \ OE)$ and the autophagy deficient mutants atg2 and atg5 were sensitive to salt. (B) Seed germination rates in (A). Approximately 300 seeds from 5-6 plates of three biological replicates were quantified. (C, D) statistics of seedlings with fully expanded first pair of true leaves (growth stage 1.02) in (A). (E) TEM of mesophyll cells from true leaves of 12-day-old seedlings with or without 150 mM NaCl treatment (0.5 h). mtm2 has healthy-looking chloroplasts even after salt stress, and chloroplasts in WT became swollen with defective thylakoids and accumulated plastoglobules. (F) Statistics of the number of normal and swelling chloroplasts in (D), n > 50 for each genotype. (G) Heat map showing the changes of transcript levels of photosynthesis-related genes in WT and mtm2 before and after salt stress. ROPA, ROPB, and ROPC1/ROPC2. (H) heat map showing the changes of transcript levels of photosynthesis-related genes in WT and mtm2 before and after salt stress. Each grid represents the \log_2 (FPKM) value normalized to that of WT before stress. (I) CoroNa green staining of Na⁺ in the cortex cells at the root tips of 5-day-old WT, mtm2, and atg2, with or without 100 mM NaCl treatment (8 h). CoroNa green accumulated in the vacuoles of mtm2 especially after salt stress. atg2 was used as a negative control, and the plasma membrane was stained with FM 4-64. Bar: 20 μ m. (J) Quantification of the fluorescence intensity of CoroNa green in (I), n > 50 cells for each. (K) Heat map showing changes of transcript levels of transporters involved in salt stress adaptation in WT and mtm2 before and after salt stress (150 mM NaCl, 1 h). Each grid represents the \log_2 (FPKM) value normalized to that of WT befor

We proposed a model to describe the cellular function of MTM2 (Figure S7J). Under normal growth conditions, MTM2 safeguards the level of autophagy by hydrolyzing PtdIns3P upstream of PtdIns3P effectors, such as ATG18–ATG2 complex and the conjugation systems. Upon salt stress, MTM2 is upregulated at both transcript and protein level after the initial boost of autophagic flux, to prevent excessive high levels of autophagy. Mechanistically, the multivalent interaction between MTM2 and

SEC23A likely inhibits the budding of COPII vesicles, which are a known membrane source for autophagosome formation.

Discussion

In this study, we identify Myotubularin 2 of Arabidopsis as a specific inhibitor of autophagy. MTM2 inhibits autophagy induction by de-phosphorylating PtdIns3P at ERES (Figures 1, 4), thus leads to abnormal accumulation of core ATG proteins downstream of PtdIns3P and a complete inhibition of autophagic flux (Figure 3). Conversely, knockout of MTM2 leads to induction of basal level, selective, TOR inhibition-induced, and salt stress-induced autophagy (Figure 2). Importantly, MTM2 is specific for autophagy inhibition, since none of the endolysosomal trafficking events examined other than autophagy is affected in mtm2 (Figure S4). Besides, apart from ATG14 of PtdIns3K (Figure 3), MTM2 only colocalizes with COPII inner and outer coat proteins, and is wrapped by SEC16A, the defining protein for ERES, but not to Golgi, TGN, or the tonoplast (Figure 4, Movie S1-5, Figure S3). Meanwhile, its proximal proteome only included ER-to-Golgi trafficking components as an enriched GO cellular component (Figure 4). Experimental and computational PPI analysis showed that MTM2 interacts with the COPII inner coat protein SEC23A with its phosphatase (PTP) domain (Figure 5, Figure S5). Overexpression of MTM2 blocks secretion of certain cargo proteins from ERES, and knockout of MTM2 promotes protein secretion (Figure 6), suggesting that MTM2 inhibits COPII-mediated ER-to-Golgi trafficking (Figure S7J). The fact that MTM2 inhibits both PtdIns3Pmediated autophagosome biogenesis and COPII-mediated ERto-Golgi transport suggested that the two processes may be spatiotemporally tightly associated. Apart from the mechanism, we also described plant-specific function of MTM2 in salt stress tolerance (Figure 7, Figure S6 and 7). In salt stress conditions, the mtm2 mutant grows better, can maintain healthy chloroplasts and likely normal photosynthesis, promptly compartmentalized more Na⁺ into the vacuole, and induce and repress key genes in stress response faster than the WT. The fact that MTM2 mRNA and protein levels were induced at the same time when NaCl-induced autophagy is repressed suggested that it may be a key regulator of salt stress adaptation. In many ways mtm2 resembles salt cress, the close relative of Arabidopsis that can survive sea water. It would be interesting to see if a similar mechanism on autophagy regulation exists in salt cress, and if such a mechanism is indeed responsible for its competence.

To our knowledge, this study is the first to find a myotubularin of any eukaryotes at ERES. More than three decades of studies on PtdIns3P have come to a consensus that it defines the endosomal functions. Before any vesicle can leave the territory of endosomes, PtdIns3P turnover is required [13]. Meanwhile, overaccumulation of PtdIns3P leads to defective organization of the ER, which is a distinct phenotype of human MTM1 mutation [85]. Hence the PtdIns3P-enriched ER subdomain that scaffolds phagophore assembly is very special. One can speculate that both PtdIns3K and PI-3-phosphatase activity is required to adjust the timing and the time span of phagophore formation. We showed that this PI-3-phosphtase is MTM2 in Arabidopsis. It is likely that some animal MTMs that have been characterized as negative regulator of autophagy may carry out a similar function, and some may also appear at ERES. The fact that the single MTM of yeast mainly facilitates release of Atg proteins from the mature autophagosome to enable their fusion to the vacuole suggested that the primary/earliest function of MTM is to antagonize the endo-lysosomal function of PtdIns3K, which is more critical to cell survival. It is possible that other PI phosphatases that have overlapping functions with Ymr1 May inhibit autophagosome assembly in yeast, or the emergence of Ymr1 at the PAS may be too transient to capture since Ymr1 seldom forms puncta.

In animals, omegasome is derived from PtdIns3Penriched ER subdomains and serves as a precursor or a platform for phagophore expansion [86]. In Arabidopsis, the PtdIns3P-binding BAR-domain protein SH3P2 participates in phagophore assembly, and some phagophore labeled by SH3P2 appeared to derive from the ER [87]. The Arabidopsis ATG5 defines a toroidal domain on the expanding phagophore and leaves the phagophore upon its detachment from the ER [57]. A lipid transfer protein, ORP2A, resides at the ER-autophagome membrane contact site [88]. RNA-interference of ORP2A led to PtdIns3P accumulation in the ER and autophagy inhibition [88]. It is possible that MTM2 work together with SH3P2 or ORP2A in phagophore assembly. In this study, we were limited by the low expression level of MTM2, and had to rely on overexpression of MTM2, driven by a UBQ10 promoter, to study its subcellular localization, and how it may affect autophagosome formation. Overexpression of a PI-3-phosphatase, even if it specifically localizes to one subcellular structure, may still affect the level and distribution of intracellular PtdIns3P. The enlarged ATG8a, ATG18a, and ATG5 puncta, resulting from MTM2 overexpression in both N. benthamiana and Arabidopsis, may be aggregates that failed to assemble autophagosome. Alternatively, they could be enlarged autophagosomes that cannot seal due to lack of PtdIns3P required for ESCRT function. They could even be sealed enlarged autophagosomes that fail to fuse with MVB or vacuole due to lack of PtdIns3P required for fusion. Hence these enlarged puncta could be artifacts caused by ectopic expression of MTM2. How MTM2 May function with other known players at the initial stage of autophagosome formation needs future exploration.

The fact that many salt- and osmotic-responsive transporters have higher transcript levels in unstressed mtm2 indicated that upregulation of COPII-mediated secretion of transporters may represent a general strategy for acute abiotic stress tolerance. Specificity may exist at the level of COPII vesicle assembly. Several transporters induced in mtm2 have been characterized as cargoes of ABA-induced giant COPII vesicles [78], suggesting that MTM2 May also be involved in the formation of these stress-specific COPII vesicles. The fact that MTM2 only interacted with SEC23A again validated the functional divergence of plant COPII components. How MTM2 transcription is induced by salt stress, and which E3 ligase may target MTM2 for ubiquitin 26S proteasome degradation is currently unknown. Also, we do not know which transporters are critical for sodium ion accumulation in the vacuole. Nevertheless, our findings revealed that, by specifically enhancing PtdIns3P-mediated autophagosome formation and likely COPII-mediated secretion at the same time, plants that are tolerant to salt stress can be generated.



Materials and methods

Accession numbers

MTM2 (AT5G04540), ATG14b (AT4G08540), ATG13a (AT3G49590), ATG2 (AT3G19190), ATG5 (AT5G17290), (AT4G21980), ATG8b (AT4G04620), ATG8c (AT1G62040), ATG8d (AT2G05630), ATG8e (AT2G45170), ATG8f (AT4G16520), ATG8g (AT3G60640), ATG8h (AT3G06420), ATG8i (AT3G15580), ATG9 (AT2G31260), ATG18a (AT3G62770), ATG18b (AT4G30510), ATG18h (AT1G54710), Derlin1 (AT4G29330), SEC23A (AT4G01810), SEC23B (AT1G05520), SEC23E (AT3G23660), SEC24A (AT3G07100), SEC13A (AT2G30050), SEC31A (AT1G18830), SEC31B (AT3G63460), SEC16A (AT5G47480), SAR1B (AT1G56330), SAR1D (AT3G62560), MTM1 (AT3G10550), VPS38 (AT2G32760), TIP4;1 (AT2G25810).

Plant materials and growth conditions

T-DNA insertion lines mtm2(SALK_147282), atg2 (SALK 076727), (SAIL 129 B07), atg5 mtm1(SALK 029185), vps38 (SAIL 552 F02) were obtained from the Arabidopsis Biological Resource Center (ABRC). PIN2: PIN2-GFP was a gift from Dr. Ben Scheres (Wageningen University) and Dr. Shuzhen Men (Nankai University), the 12S and 2S antibodies were a gift from Dr. Ikuko Hara-Nishimura (Konan University), and secGFP seeds were a gift from Dr. Xu Yan and Dr. Jianwei Pan (Lanzhou University). All mutants were verified by genomic PCR and RT-PCR. The double mutants were generated by crossing and confirmed by genomic PCR in F2 population. GFP-ATG8a lines in mtm2, mtm2/ProMTM2:MTM2-GFP and atg5 background were obtained by crossing with WT/GFP-ATG8a.

Generally, Arabidopsis thaliana (ecotype Columbia-0, Col-0) seeds were surface-sterilized with 75% ethanol for 5 min, rinsed with ddH₂O for five times, then stratified at 4°C for 2 days before plated on 1/2 Murashige and Skoog (1/2 MS) medium (Duchefa, M0222) containing 0.8% (w:v) agar, 1% (w:v) sucrose, pH 5.7. The plants were then kept at a 16 h $(22^{\circ}C)/8 h$ dark (18°C) photoperiod a photosynthetic photon flux density at 120 μE m⁻² sec⁻¹ in a growth room. Soil-grown plants were kept under the same conditions.

For liquid culture, same counts of sterilized and stratified seeds were put into flasks containing liquid 1/2 MS, and grown with gentle shaking (80-100 rpm). At day 10, seedlings were transferred to fresh liquid 1/2 MS (Control), 1/2 MS without nitrogen (-N), 1/2 MS without sucrose plus kept in the dark (-C), and let grown for indicated period of time. Carbon starvation on plate was performed as described [54,89].

For the salt-tolerance phenotype observation, sterilized seeds were stratified for 2 days on solid 1/2 MS medium. Then the plates were kept horizontally in the growth room for 10 days. To observe the fluorescence of secGFP, four-dayold seedlings were transferred to 1/2 MS plates, pH 8.1, and imaged 3 days later [79].

Nicotinana benthamiana seeds were sown in peat soil (Klasmann-Deilmann TS1, 876) and one-week-old seedlings were transplanted carefully to new pots with one plant per pot (10 cm in diameter). Generally, 3- to 4-week-old N. benthamiana plants were used for transient expression of recombinant proteins.

Plasmid construction

For transient and stable transformation, full length cDNAs or genomic DNA were fused in-frame with GFP, dsRed, mRuby, or BFP tags under the control of the UBQ10 promoter, in modified pCAMBIA vectors (Abcam, ab275753; deposited by Qingqiu Gong). For BiFC assay, CDS of MTM2 and other bait proteins were inserted into Pro35S:cEYFP and Pro35S:nEYFP respectively, at NcoI restriction sites using a homologous recombination kit (Vazyme, C112-02). All constructs were verified by DNA sequencing.

RT-PCR, quantitative RT-PCR (Q-RT-PCR)

RNA extraction, reverse transcription, RT-PCR and Q-RT-PCR were done as described [90]. All primers used for PCR and constructs are listed in Table S2.

Plant transformation

To generate Arabidopsis transgenic lines, constructs were introduced into Agrobacterium tumefaciens (GV3101) for floral dipping [91]. Primary transformants were selected by antibiotic resistance and further verified by PCR and immunoblotting. Individual T2 and T3 lines were used. Transient transformation was done as described [92] on N. benthamiana leaves.

Protein extraction and immunoblotting

Protein extraction was done as described [49]. Western blotting was done as described [90]. Primary antibodies used include anti-GFP (1:5000 dilution; Utibody, UM3002), anti-BFP (1:5000 dilution; Evrogen, AB233), anti-MBP (1:5000 dilution; Utibody, UM3008), anti-His (1:5000 dilution; Utibody, UM3006), anti-GST (1:5000 dilution; Sungene Biotech, KM8005), anti-NBR1 (1:10000 dilution; Agrisera, AS14 2805A), anti-MTM2 (1:1000 dilution), anti-Histone H3 (1:10000 dilution; ABclonal, A2348), anti-Actin (1:5000 dilution; Sungene Biotech, KM9004), and the appropriate IgG-HRP-conjugated secondary antibody (1:5000; ZSGB-Bio, ZB-2301 and 2305). Anti-MTM2 was generated toward a synthetic peptide RNGDCTVEVEDG of MTM2 (aa 739-750) in rabbits at Peking University Health Science Centre, Beijing, China. The signal was developed using Highly Sensitive ECL Chemiluminescence Substrate (Vazyme, E412-02) and detected using a chemiluminescent western blot scanner (ChemiScope 6100T, Clinx, China). All experiments were repeated at least 3 times, and one representative result was shown.

For GFP-ATG8a cleavage assay (autophagic flux), fourteen-day-old seedlings were treated with 1 µM AZD8055

(Selleck, S1555) for 2 h. For the detection of NBR1, seedlings were treated with 1 µM AZD8055 and/or 100 µM E64d (Selleck, S7393) for 2 h, 150 mM NaCl and 0.5 µM ConA for 30 min. ProUBQ10:GFP-MTM2 seedlings were treated with 150 mM NaCl, 50 μM cycloheximide (CHX; Selleck, S7418), and 50 µM MG132 (Selleck, S2619), respectively.

Secreted protein extraction was done as described [93]. Seed storage protein extraction and immunoblotting of 2S albumin and 12S globulin was done as described previously [94].

Protein lipid overlay assay

The PH-GRAM domain (residues 45-161) and the PH-GRAM-Myotub-related-PTP domains (residues 45-491) of MTM2 were PCR-amplified and inserted into BamH I and Xho I sites of pGEX-6P-2 to generate GST-PH-GRAM and GST-Myotub-related-PTP fusion constructs. The recombinant proteins were expressed in E. coli (BL21) and purified with GSTrap FF columns (GE Healthcare, GE17-5130-01) following manufacturer's instructions. Protein-lipid overlay assays were done on PIP Array (Echelon, p-6100) membranes following manufacturer's instructions. Anti-mouse HRP secondary antibody (Sungene, LK2003L) was used at 1:10000, and the signal was detected with a Chemiluminescent detection kit (Millipore, WBAVDCH01).

Protein lipid Co-floatation assay

The recombinant protein His-MBP- MTM2 aa 42-161 (PH-GRAM domain) was expressed in E. coli (BL21 DE3) and purified with Ni-NTA beads (Smart-lifesciences, SA005100), purified protein was centrifuged to remove beads and protein aggregates before concentration was determined.

Each lipid from lipid stocks in organic solvent were mixed into glass tubes. The lipid composition is POPC:POPE: PtdIns3P:rhodamine DHPE (67:26:6:1) (Avanti, 850457P, 850757P, 850150P, 810104P). The solvent was evaporated under a stream of nitrogen gas in a fume hood, and then transferred to a vacuum desiccator overnight. Vesicle buffer (20 mM HEPES, pH 7.5, 90 mM NaCl, 1 mM TCEP [MedChemExpress, HY-W011500]) was added to obtain a final lipid concentration of 1 mM. Hydrated lipids were vortexed for 5 min and passed through in a lipid extruder to generate 100 nm liposomes.

Liposomes and protein were mixed to final concentrations of 1 mM and 1 µM, respectively, incubated with rotation at 4°C for 1 h, and then was mixed gently with vesicle buffer containing 70% histodenz (Sigma, D2158), which provided a histodenz concentration of 40%. The vesicle buffer containing 35%, 30%, and 0% histodenz were carefully covered on top of the above solution in sequence. Samples were centrifuged at 48,000 rpm for 4 h at 4°C using a swinging-bucket rotor SW 55 Ti (Beckman, Germany). The top and bottom fraction of samples were carefully collected, mixed with SDS-PAGE loading buffer, and boiled at 100°C for 8 min for immunoblotting.

Co-immunoprecipitation and affinity-isolation assay

For co-immunoprecipitation, GFP-SEC23A and MTM2dsRed were co-expressed in N. benthamiana leaves, and proteins were extracted with IP lysis buffer (50 mM Tris-HCl, pH 7.5, 150 mM NaCl, 1 mM MgCl₂, 20% glycerol, 0.2% NP-40 [Sangon Biotech, A600385], and 1× protease inhibitor [Selleck, B14001]) by vortexing, then centrifuged at 13,000 \times g at 4°C for 10 min. The supernatant was incubated with GFPbeads for 3 h at 4°C, beads were collected and washed 5 times with washing buffer (50 mM Tris-HCl, pH 7.5, 150 mM NaCl, 1 mM MgCl₂, 20% glycerol, 0.01% NP-40), then mixed with SDS-PAGE loading buffer and boiled at 100°C for 8 min for immunoblotting.

For prokaryotic expression and affinity-isolation assay, constructs were introduced into E. coli strain BL21 (DE3). Protein synthesis was induced with 0.3 mM IPTG (Beyotime, ST098) at 16°C for 12 h, collected by centrifugation at 13,000 × g for 20 min and resuspended in binding buffer (50 mM Tris-HCl, pH 8.0, 500 mM NaCl, 1 mM PMSF [Sangon Biotech, A100754]). After co-sonication and co-incubation of the centrifuged supernatant, GST agarose beads (Beyotime, P2251) or MBP agarose beads (GE Healthcare 28,936,640-AB) were added in for continued incubation for 2 h. The beads were then washed 8 times with washing buffer (50 mM Tris-HCl, pH 8.0, 500 mM NaCl), mixed with SDS-PAGE loading buffer, and boiled at 100°C for 8 min for immunoblotting.

Laser scanning confocal microscopy (LSCM)

Lower leaf epidermal cells of N. benthamiana leaves after 36-48 h of agrobacterium infiltration were imaged with a Ni-E A1 HD25 confocal microscope (Nikon, Japan).

To quantify the number of autophagosomes, five-day-old proUBQ10:GFP-ATG8a Arabidopsis seedlings were treated with 1/2 MS or 1/2 MS containing 150 mM NaCl and 0.5 μM concanamycin A (APExBIO, A8633) for 30 min. Then cells in the root transition zone were scanned with Nikon A1 with 1 μm interval in a total volume of $215 \times 215 \times 20 \,\mu m^3$. The number of GFP puncta in each cell vacuole in the 3D field of view was counted. For each condition, at least 30 seedlings from five biological replicates were imaged, and > 20 cells were quantified for the numbers of autophagosomes/autophagic bodies. For colocalization of MTM2 and SEC23A in Arabidopsis, time-lapse images/movies were captured with a spinning disc confocal IXplore SpinSR (Olympus, Japan).

To observe endocytosis, five-day-old seedlings were stained for 5 min with 8 µM FM 4-64 (Thermo Fisher Scientific, F34653) on ice, rinsed with water for three times. Cortical cells in the root transition zone were imaged at indicated period of time, and at least 30 seedlings from three biological replicates were imaged.

Endocytosis of the early endosome and exocytosis of the recycling endosome was examined by observing formation of brefeldin A (BFA) bodies and washout of BFA bodies. Fourday-old PIN2-GFP seedlings were pretreated with 1/2 MS liquid medium containing 50 µM CHX for 2 h, then transferred to 1/2 MS containing 50 µM BFA (Selleck, S7046) plus

CHX for 30, 60, and 90 min, respectively, and scanned with the Nikon confocal microscope. The seedlings treated with BFA for 90 min were then transferred to 1/2 MS containing CHX for 30 min for BFA washout. At least 20 roots were measured from three biological replicates, about cortical 40 cells in the root transition zone from seven different roots were measured. For dark-induced vacuolar transport and degradation of PIN2, five-day-old seedlings were stained with FM 4-64 on ice for 5-10 min. Then the excess dye was washed off, and the seedlings were imaged immediately (time 0 h), or incubated for 2 and 4 h in the dark before scanning. Images were collected from at least 30 roots from three biological replicates, and representative images were shown.

The GFP fluorescence signal was excited at 488 nm and emission was collected at 500-550 nm, mRuby and dsRed was excited at 561 nm and emission was collected at 570-620 nm. BFP was excited at 405 nm and emission was collected at 425-475 nm. FM 4-64 was excited at 561 nm and emission was collected at 665-740 nm. CoroNa Green was excited at 488 nm and emission was collected at 500-550 nm.

Predicting the 3D structure of MTM2-SEC23A complex

AlphaFold [95] was used to predict the monomer structures of MTM2 and SEC23A, and AlphaFold-Multimer [96] was used to predict the binding complex of MTM2-SEC23A with multiple sequence alignments (MSA) searching option set as all genetics database of v2.2.0. Due to the absurd chaincrossing structures produced by AlphaFold-Multimer, the predicted structure with the highest model confidence score was selected for further optimization using the proteinprotein docking [97,98] and protein structure relax [99,100] protocols of Rosetta. During the protein-protein docking protocol, the monomer structures of MTM2 and SEC23A were aligned to the complex structure to create the initial structure. All the Rosetta simulations were performed under the ref2015_cart [101] scoring function, and the other options were set as default. The 300 and 10 structures were separately produced by protein-protein docking and relax protocol. Finally, all the resulting complex structures were evaluated by visual inspection and the (MM/GBSA) binding energy calculation. The MM/GBSA were calculated by the prime MM-GBSA module of Schrödinegr2021-1 with the OPLS4 force field.

TurboID and mass spectrometry analysis

Four-week-old N. benthamiana leaves were infiltrated with agrobacteria carrying a TurboID-GFP-MTM2 construct. Thirty-six h later, infiltration solution (200 µM biotin [TCI, B0463], 10 mM MgCl₂) was infiltrated into the same leaves. The leaves were harvested 6 h later and frozen in liquid nitrogen. Protein extraction for TurboID was adapted from previous reports [102,103]. Leaf material (350 mg) was ground in liquid nitrogen, and proteins were extracted in 700 µL of chilled extraction buffer (150 mM Tris-HCl, pH 7.5, 500 mM NaCl, 0.4% SDS, 2% Triton X-100 [Sangon, TB0198], 10 mM EDTA, 15 mM DTT, 2% polyvinylpolypyrrolidone/PVPP [Sangon, P705843], 1%

proteinase inhibitor cocktail). Supernatants after centrifugation were run onto a Zeba™ Spin Desalting Column (Thermo Fisher Scientific 89,891), which was preequilibrated with protein extraction buffer (150 mM Tris-HCl, pH 7.5, 500 mM NaCl, 0.4% SDS, 2% Triton X-100, 10 mM EDTA). Protein extract was added to the column, and centrifuged at 1000 × g for 2 min at 4°C. The desalted samples were loaded to protein extraction bufferequilibrated streptavidin magnetic beads (200 µL aliquot; MedChemExpress, HY-K0208) and incubated overnight at 4°C. Wash and retrieval of beads were performed as reported [103]. After removal of supernatant, the beads were washed twice on a rotator for 8 min each with 1.7 mL of wash buffer I (2% SDS); twice with wash buffer II (50 mM HEPES, pH 7.5, 500 mM NaCl, 1 mM EDTA, 0.1% deoxycholic acid [w:v; Yeasen, 60334ES10], 1% Triton X-100); twice with wash buffer III (10 mM Tris-HCl, pH 7.4; 250 mM LiCl, 1 mM EDTA, 0.1% deoxycholic acid [w: v], 1% NP-40 [v:v]); and twice with wash buffer IV (50 mM Tris-HCl, pH 7.5). The beads were then washed six times for 5 min each with 50 mM ammonium bicarbonate buffer, pH 7.5. After removal of supernatant, the remaining beads were mixed with SDS loading buffer and boiled at 100°C.

After SDS-PAGE of protein samples, the gel was stained with Coomassie Brilliant Blue (CBB), and bands were cut into small blocks (<5 mm²) and put in RNase-free tubes for treatment before mass spectrometry. Tryptic peptides were analyzed on Nano liquid chromatography-quadrilateral rail trap mass spectrometer (Instrumental analysis center, Shanghai Jiao Tong University). Peptide sequences and UniProt ID were retrieved. Protein enrichment analysis was conducted on Metascape [104], and the top 10 enriched terms were illustrated with Cytoscape ClueGO [105].

Transmission electron microscopy (TEM)

Sections ($\sim 1 \times 3$ mm) cut from the central parts of euphyllas of 12-day-old seedlings were fixed in 2.5% (v:v) glutaraldehyde overnight, then post-fixed in 1% OsO₄ (w:v) for 2 h. After fixation, samples were rinsed 3 times in 0.1 M phosphate buffer (Na₂HPO₄, NaH₂PO₄, pH 6.8). After dehydration with alcohol and acetone series, samples were embedded in EPON 812 (Ted pella 18,010). Ultrathin sections (thickness 70 nm) were cut with a Leica EM UC7 (Leica, Germany), mounted on copper grids and contrasted with TI Blue stainer (Nisshin EM, GN335) and 3% lead citrate solution. The sections were visualized with a Tecnai G2 spirit Biotwin TEM (FEI, USA) at 120 kV accelerating voltage.

CoroNa green and GUS Staining

For CoroNa Green staining, five-day-old seedlings were immersed in liquid 1/2 MS or 1/2 MS containing 100 mM NaCl for 6 h, then transferred to each of the two solutions containing 5 µM CoroNa Green (Thermo Fisher Scientific, C36676). Two h later the seedlings were washed 3 times and stained with 8 µM FM 4-64 on ice for 5 min, then washed again before imaging. Confocal images were captured from > 30 seedlings from three biological replicates.

For GUS staining, eight-day-old T3 seedlings (growth stage 1.02) carrying ProMTM2:GUS were immersed in liquid 1/2 MS or 1/2 MS containing 150 mM NaCl for 6 h, stained with GUS staining solution (0.5 g/L X-gluc [Yeasen, 10904ES03], 0.5 mM K₃Fe[CN]₆, 0.5× PBS [Cellgro, 21–040-CV], 0.5 mM K₄Fe[CN]₆, 0.1% [v:v] Triton X-100) for 6 h, washed with decolorizing solution (Ethanol:acetic acid, 3:1), and photographed. Three biological replicates were done (>10 seedlings each), and representative results are shown.

Chlorophyll content was measured and calculated as described previously [106].

Statistical analysis

Statistical analyses were performed using GraphPad Prism 8 (GraphPad Software). Data were presented as mean \pm SEM (Standard error of the mean) and statistical significance was analyzed by two-sided Student's t-test and Tukey's test (*p < 0.05, **p < 0.01, ****p < 0.001, ****p < 0.0001) using the SPSS and GraphPad. The colocalization relationship of two fluorescent signals and quantitative statistics of bolt bands was quantified using the ImageJ (http://rsb.info.nih.gov/ij), Pearson's and Mander's coefficients were calculated using colocalization plugin of ImageJ.

RNA sequencing and transcriptome analysis

For the transcriptome analysis, fourteen-day-old, vertically grown WT and *mtm2* seedlings were immersed in liquid 1/2 MS with or without 150 mM NaCl for 1 h, frozen in liquid nitrogen and stored at -80°C. Two independent replicates were performed. All samples were analyzed by GENEWIZ Co., Ltd, China, with deep sequencing performed on an Illumina Hiseq 2500 platform (Illumina, USA), generating over 40 million reads of high-quality Illumina bases for each sample. The RNA-sequencing data have been deposited to the SRA database under the bioproject ID PRJNA918539.

Functional ontology analysis for the genes upregulated for more than 2-fold before and after salt treatment in *mtm2* were conducted on Metascape (https://metascape.org/gp), and the annotation terms of Biological Process (BP), Cellular Component (CC), and Molecular Function (MF) were selected and drawn to pictures by an R package, ggplot2. The log₂ (FPKM) values were put into software GraphPad Prism to generate a heat map.

Acknowledgements

We thank Ben Scheres (Wageningen University) and Shuzhen Men (Nankai University) for the gift of PIN2-GFP seeds, Xu Yan and Jianwei Pan (Lanzhou University) for secGFP seeds, Ikuko Hara-Nishimura (Konan University) for anti-2S and anti-12S antibodies, Harald Stenmark (University of Oslo) for 2×FYVE plasmid, Haoxin Xu (Zhejiang University) for 2×ML1N plasmid, and Ms. Qian Luo from Core Facility and Technical Service Center (Shanghai Jiao Tong University) for help with imaging. We also thank Yixian Cui (Wuhan University), Junjie Hu (Institute of Biophysics, Chinese Academy of Sciences), Qing Lu (Shanghai Jiao Tong University), Juan Wang (Beijing University of Technology), and Zhiping Xie (Shanghai Jiao Tong University) for suggestions.

Disclosure statement

No potential conflict of interest was reported by the author(s).

Funding

The work was supported by the National Natural Science Foundation of China [92354302, 91954102, 32270726, 31871355]; Natural Science Foundation of Shanghai [23ZR1429400].

Data availability statement

The RNA-sequencing data that support the findings of this study are openly available in the SRA database under the bioproject ID PRJNA918539.

ORCID

Qingqiu Gong (b) http://orcid.org/0000-0002-9803-8554

References

- [1] Morishita H, Mizushima N. Diverse cellular roles of autophagy. Annu Rev Cell Dev Biol. 2019;35(1):453–475. doi: 10.1146/annurev-cellbio-100818-125300
- [2] Signorelli S, Tarkowski LP, Van den Ende W, et al. Linking autophagy to Abiotic and biotic stress responses. Trends Plant Sci. 2019;24(5):413–430. doi: 10.1016/j.tplants.2019.02.001
- [3] Nishimura T, Tooze SA. Emerging roles of ATG proteins and membrane lipids in autophagosome formation. Cell Discov. 2020;6(1):32. doi: 10.1038/s41421-020-0161-3
- [4] Xie Z, Klionsky DJ. Autophagosome formation: core machinery and adaptations. Nat Cell Biol. 2007;9(10):1102–1109. doi: 10. 1038/ncb1007-1102
- [5] Olivas TJ, Wu Y, Yu S, et al. ATG9 vesicles comprise the seed membrane of mammalian autophagosomes. J Cell Biol. 2023;222 (7). doi: 10.1083/jcb.202208088
- [6] Orsi A, Razi M, Dooley HC, et al. Dynamic and transient interactions of Atg9 with autophagosomes, but not membrane integration, are required for autophagy. Mol Biol Cell. 2012;23 (10):1860–1873. doi: 10.1091/mbc.e11-09-0746
- [7] Sawa-Makarska J, Baumann V, Coudevylle N, et al. Reconstitution of autophagosome nucleation defines Atg9 vesicles as seeds for membrane formation. Science. 2020;369(6508). doi: 10.1126/ science.aaz7714
- [8] Graef M, Friedman JR, Graham C, et al. ER exit sites are physical and functional core autophagosome biogenesis components. Mol Biol Cell. 2013;24(18):2918–2931. doi: 10.1091/mbc.e13-07-0381
- [9] Shima T, Kirisako H, Nakatogawa H. COPII vesicles contribute to autophagosomal membranes. J Cell Biol. 2019;218(5):1503–1510. doi: 10.1083/jcb.201809032
- [10] Chung KP, Zeng Y, Jiang L. COPII paralogs in plants: functional redundancy or diversity? Trends Plant Sci. 2016;21(9):758–769. doi: 10.1016/j.tplants.2016.05.010
- [11] Li B, Zeng Y, Jiang L. COPII vesicles in plant autophagy and endomembrane trafficking. FEBS Lett. 2022;596(17):2314–2323. doi: 10.1002/1873-3468.14362
- [12] Zeng Y, Li B, Ji C, et al. A unique AtSar1D-AtRabD2a nexus modulates autophagosome biogenesis in Arabidopsis thaliana. Proc Natl Acad Sci USA. 2021;118(17). doi: 10.1073/pnas. 2021293118
- [13] Posor Y, Jang W, Haucke V. Phosphoinositides as membrane organizers. Nat Rev Mol Cell Biol. 2022;23(12):797–816. doi: 10. 1038/s41580-022-00490-x
- [14] Kihara A, Noda T, Ishihara N, et al. Two distinct Vps34 phosphatidylinositol 3-kinase complexes function in autophagy and carboxypeptidase Y sorting in Saccharomyces cerevisiae. J Cell Biol. 2001;152(3):519–530.



- [15] Obara K, Sekito T, Niimi K, et al. The Atg18-Atg2 complex is recruited to autophagic membranes via phosphatidylinositol 3-phosphate and exerts an essential function. J Biol Chem. 2008;283(35):23972-23980. doi: 10.1074/jbc.M803180200
- [16] Dove SK, Piper RC, McEwen RK, et al. Svp1p defines a family of phosphatidylinositol 3,5-bisphosphate effectors. Embo J. 2004;23 (9):1922–1933. doi: 10.1038/sj.emboj.7600203
- [17] Kotani T, Kirisako H, Koizumi M, et al. The Atg2-Atg18 complex tethers pre-autophagosomal membranes to the endoplasmic reticulum for autophagosome formation. Proc Natl Acad Sci USA. 2018;115(41):10363-10368. doi: 10.1073/pnas.1806727115
- [18] Maeda S, Otomo C, Otomo T. The autophagic membrane tether ATG2A transfers lipids between membranes. Elife. 2019;8:e45777.
- [19] Valverde DP, Yu S, Boggavarapu V, et al. ATG2 transports lipids to promote autophagosome biogenesis. J Cell Biol. 2019;218 (6):1787-1798. doi: 10.1083/jcb.201811139
- [20] Matoba K, Kotani T, Tsutsumi A, et al. Atg9 is a lipid scramblase that mediates autophagosomal membrane expansion. Nat Struct Mol Biol. 2020;27(12):1185-1193. doi: 10.1038/s41594-020-00518-w
- [21] Gomez-Sanchez R, Rose J, Guimaraes R, et al. Atg9 establishes Atg2-dependent contact sites between the endoplasmic reticulum and phagophores. J Cell Biol. 2018;217(8):2743-2763. doi: 10. 1083/jcb.201710116
- [22] Juris L, Montino M, Rube P, et al. PI3P binding by Atg21 organises Atg8 lipidation. Embo J. 2015;34(7):955-973. doi: 10.15252/ embj.201488957
- [23] Dooley HC, Razi M, Polson HE, et al. WIPI2 links LC3 conjugation with PI3P, autophagosome formation, and pathogen clearance by recruiting Atg12-5-16L1. Mol Cell. 2014;55(2):238-252. doi: 10.1016/j.molcel.2014.05.021
- Dudley LJ, Cabodevilla AG, Makar AN, et al. Intrinsic lipid binding activity of ATG16L1 supports efficient membrane anchoring and autophagy. Embo J. 2019;38(9). doi: 10.15252/embj. 2018100554
- [25] Nascimbeni AC, Codogno P, Morel E. Phosphatidylinositol-3-phosphate in the regulation of autophagy membrane dynamics. FEBS J. 2017;284(9):1267-1278. doi: 10.1111/febs.13987
- [26] Zhou X, Wang L, Hasegawa H, et al. Deletion of PIK3C3/Vps34 in sensory neurons causes rapid neurodegeneration by disrupting the endosomal but not the autophagic pathway. Proc Natl Acad Sci USA. 2010;107(20):9424–9429. doi: 10.1073/pnas.0914725107
- [27] Welters P, Takegawa K, Emr SD, et al. AtVPS34, a phosphatidylinositol 3-kinase of Arabidopsis thaliana, is an essential protein with homology to a calcium-dependent lipid binding domain. Proc Natl Acad Sci USA. 1994;91 (24):11398-11402. doi: 10.1073/pnas.91.24.11398
- [28] Laporte J, Blondeau F, Buj-Bello A, et al. Characterization of the myotubularin dual specificity phosphatase gene family from yeast to human. Hum Mol Genet. 1998;7(11):1703-1712. doi: 10.1093/ hmg/7.11.1703
- [29] Parrish WR, Stefan CJ, Emr SD. Essential role for the myotubularin-related phosphatase Ymr1p and the synaptojanin-like phosphatases Sjl2p and Sjl3p in regulation of phosphatidylinositol 3-phosphate in yeast. Mol Biol Cell. 2004;15 (8):3567-3579. doi: 10.1091/mbc.e04-03-0209
- Cebollero E, van der Vaart A, Zhao M, et al. Phosphatidylinositol-3-phosphate clearance plays a key role in autophagosome completion. Curr Biol. 2012;22(17):1545-1553. doi: 10.1016/j. cub.2012.06.029
- [31] Kim SA, Vacratsis PO, Firestein R, et al. Regulation of myotubularin-related (MTMR)2 phosphatidylinositol phosphatase by MTMR5, a catalytically inactive phosphatase. Proc Natl Acad Sci USA. 2003;100(8):4492-4497. doi: 10.1073/pnas.0431052100
- [32] Zou J, Zhang C, Marjanovic J, et al. Myotubularin-related protein (MTMR) 9 determines the enzymatic activity, substrate specificity, and role in autophagy of MTMR8. Proc Natl Acad Sci USA. 2012;109(24):9539-9544. doi: 10.1073/pnas.1207021109
- [33] Taguchi-Atarashi N, Hamasaki M, Matsunaga K, et al. Modulation of local PtdIns3P levels by the PI phosphatase

- MTMR3 regulates constitutive autophagy. Traffic. 2010;11 (4):468-478. doi: 10.1111/j.1600-0854.2010.01034.x
- [34] Vergne I, Roberts E, Elmaoued RA, et al. Control of autophagy initiation by phosphoinositide 3-phosphatase jumpy. Embo J. 2009;28(15):2244-2258. doi: 10.1038/emboj.2009.159
- [35] Chua JP, Bedi K, Paulsen MT, et al. Myotubularin-related phosphatase 5 is a critical determinant of autophagy in neurons. Curr Biol. 2022;32(12):2581-2595.
- [36] Allen EA, Amato C, Fortier TM, et al. A conserved myotubularin-related phosphatase regulates autophagy by maintaining autophagic flux. J Cell Biol. 2020;219(11). doi: 10.1083/jcb. 201909073
- [37] Ketel K, Krauss M, Nicot AS, et al. A phosphoinositide conversion mechanism for exit from endosomes. Nature. 2016;529 (7586):408-412. doi: 10.1038/nature16516
- [38] Fetalvero KM, Yu Y, Goetschkes M, et al. Defective autophagy and mTORC1 signaling in myotubularin null mice. Mol Cell Biol. 2013;33(1):98-110. doi: 10.1128/MCB.01075-12
- [39] Ding Y, Ndamukong I, Zhao Y, et al. Divergent functions of the myotubularin (MTM) homologs AtMTM1 and AtMTM2 in Arabidopsis thaliana: evolution of the plant MTM family. Plant J. 2012;70(5):866-878. doi: 10.1111/j.1365-313X.2012.04936.x
- [40] Begley MJ, Dixon JE. The structure and regulation of myotubularin phosphatases. Curr Opin Struct Biol. 2005;15(6):614-620. doi: 10.1016/j.sbi.2005.10.016
- [41] Berger P, Schaffitzel C, Berger I, et al. Membrane association of myotubularin-related protein 2 is mediated by a pleckstrin homology-gram domain and a coiled-coil dimerization module. Proc Natl Acad Sci USA. 2003;100(21):12177-12182. doi: 10.1073/ pnas.2132732100
- [42] Li X, Wang X, Zhang X, et al. Genetically encoded fluorescent visualize intracellular phosphatidylinositol 3,5-bisphosphate localization and dynamics. Proc Natl Acad Sci USA. 2013;110(52):21165-21170. doi: 10.1073/pnas.1311864110
- [43] Gillooly DJ, Morrow IC, Lindsay M, et al. Localization of phosphatidylinositol 3-phosphate in yeast and mammalian cells. Embo J. 2000;19(17):4577-4588.
- Vermeer JE, van Leeuwen W, Tobena-Santamaria R, et al. Visualization of PtdIns3P dynamics in living plant cells. Plant J. 2006;47(5):687-700.
- [45] Wang J, Cai Y, Miao Y, et al. Wortmannin induces homotypic fusion of plant prevacuolar compartments. J Exp Bot. 2009;60 (11):3075-3083. doi: 10.1093/jxb/erp136
- Minina EA, Moschou PN, Vetukuri RR, et al. Transcriptional stimulation of rate-limiting components of the autophagic pathway improves plant fitness. J Exp Bot. 2018;69(6):1415-1432. doi: 10.1093/jxb/ery010
- [47] Xia T, Xiao D, Liu D, et al. Heterologous expression of ATG8c from soybean confers tolerance to nitrogen deficiency and increases yield in Arabidopsis. PLOS ONE. 2012;7(5):e37217. doi: 10.1371/journal.pone.0037217
- [48] Kim J, Lee H, Lee HN, et al. Autophagy-related proteins are required for degradation of peroxisomes in arabidopsis hypocotyls during seedling growth. Plant Cell. 2013;25(12):4956-4966. doi: 10.1105/tpc.113.117960
- [49] Luo L, Zhang P, Zhu R, et al. Autophagy is rapidly induced by salt stress and is required for salt tolerance in arabidopsis. Front Plant Sci. 2017;8:1459. doi: 10.3389/fpls.2017.01459
- [50] Zhao J, Bui MT, Ma J, et al. Plant autophagosomes mature into amphisomes prior to their delivery to the central vacuole. J Cell Biol. 2022;221(12). doi: 10.1083/jcb.202203139
- [51] Huss M, Ingenhorst G, Konig S, et al. Concanamycin A, the specific inhibitor of V-ATPases, binds to the V(o) subunit c. J Biol Chem. 2002;277(43):40544-40548. doi: 10.1074/jbc.M207345200
- [52] Chresta CM, Davies BR, Hickson I, et al. AZD8055 is a potent, selective, and orally bioavailable atp-competitive mammalian target of rapamycin kinase inhibitor with in vitro and in vivo antitumor activity. Cancer Res. 2010;70(1):288-298. doi: 10.1158/ 0008-5472.CAN-09-1751



- [53] Svenning S, Lamark T, Krause K, et al. Plant NBR1 is a selective autophagy substrate and a functional hybrid of the mammalian autophagic adapters NBR1 and p62/SQSTM1. Autophagy. 2011;7 (9):993-1010. doi: 10.4161/auto.7.9.16389
- [54] Suttangkakul A, Li F, Chung T, et al. The ATG1/ATG13 protein kinase complex is both a regulator and a target of autophagic recycling in Arabidopsis. Plant Cell. 2011;23(10):3761-3779. doi: 10.1105/tpc.111.090993
- [55] Liu F, Hu W, Li F, et al. AUTOPHAGY-RELATED14 and its associated phosphatidylinositol 3-kinase complex promote autophagy in arabidopsis. Plant Cell. 2020;32(12):3939-3960. doi: 10. 1105/tpc.20.00285
- [56] Xiong Y, Contento AL, Bassham DC. AtATG18a is required for the formation of autophagosomes during nutrient stress and senescence in Arabidopsis thaliana. Plant J. 2005;42(4):535-546. doi: 10.1111/j.1365-313X.2005.02397.x
- [57] Le Bars R, Marion J, Le Borgne R, et al. ATG5 defines a phagophore domain connected to the endoplasmic reticulum during autophagosome formation in plants. Nat Commun. 2014;5 (1):4121. doi: 10.1038/ncomms5121
- [58] Shimada T, Yamada K, Kataoka M, et al. Vacuolar processing enzymes are essential for proper processing of seed storage proteins in Arabidopsis thaliana. J Biol Chem. 2003;278 (34):32292-32299. doi: 10.1074/jbc.M305740200
- [59] Kleine-Vehn J, Leitner J, Zwiewka M, et al. Differential degradation of PIN2 auxin efflux carrier by retromer-dependent vacuolar targeting. Proc Natl Acad Sci USA. 2008;105(46):17812-17817. doi: 10.1073/pnas.0808073105
- [60] Sparkes IA, Ketelaar T, de Ruijter NC, et al. Grab a Golgi: laser trapping of Golgi bodies reveals in vivo interactions with the endoplasmic reticulum. Traffic. 2009;10(5):567-571.
- Takagi J, Kimori Y, Shimada T, et al. Dynamic capture and release of endoplasmic reticulum exit sites by Golgi Stacks in Arabidopsis. iScience. 2020;23(7):101265. doi: 10.1016/j.isci.2020.101265
- [62] McGinness AJ, Schoberer J, Pain C, et al. On the nature of the plant ER exit sites. Front Plant Sci. 2022;13:1010569. doi: 10.3389/fpls.2022. 1010569
- [63] Yang YD, Elamawi R, Bubeck J, et al. Dynamics of COPII vesicles and the Golgi apparatus in cultured nicotiana tabacum BY-2 cells provides evidence for transient association of Golgi stacks with endoplasmic reticulum exit sites. Plant Cell. (5):1513-1531. doi: 10.1105/tpc.104.026757
- [64] daSilva Ll, Snapp EL, Denecke J, et al. Endoplasmic reticulum export sites and golgi bodies behave as single mobile secretory units in plant cells. Plant Cell. 2004;16(7):1753-1771. doi: 10.1105/tpc.022673
- [65] Kim JH, Lee HN, Huang X, et al. FYVE2, a phosphatidylinositol 3-phosphate effector, interacts with the COPII machinery to control autophagosome formation in Arabidopsis. Plant Cell. 2022;34 (1):351-373. doi: 10.1093/plcell/koab263
- [66] Lee MC, Orci L, Hamamoto S, et al. Sar1p N-terminal helix initiates membrane curvature and completes the fission of a COPII vesicle. Cell. 2005;122(4):605-617.
- Zhou J, Ma J, Yang C, et al. A non-canonical role of ATG8 in Golgi recovery from heat stress in plants. Nat Plants. 2023;9 (5):749-765. doi: 10.1038/s41477-023-01398-w
- [68] Branon TC, Bosch JA, Sanchez AD, et al. Efficient proximity labeling in living cells and organisms with TurboID. Nat Biotechnol. 2018;36(9):880-887. doi: 10.1038/nbt.4201
- [69] Takagi J, Renna L, Takahashi H, et al. MAIGO5 functions in protein export from Golgi-associated endoplasmic reticulum exit sites in arabidopsis. Plant Cell. 2013;25(11):4658-4675. doi: 10. 1105/tpc.113.118158
- [70] Begley MJ, Taylor GS, Kim SA, et al. Crystal structure of a phosphoinositide phosphatase, MTMR2: insights into myotubular myopathy and charcot-marie-tooth syndrome. Mol Cell. 2003;12(6):1391-1402. doi: 10.1016/S1097-2765(03)00486-6
- [71] Bong SM, Son KB, Yang SW, et al. Crystal structure of human myotubularin-related protein 1 provides insight into the structural basis of substrate specificity. PLOS ONE. 2016;11(3):e0152611. doi: 10.1371/journal.pone.0152611

- [72] Bi X, Corpina RA, Goldberg J. Structure of the Sec23/24-Sar1 pre-budding complex of the COPII vesicle coat. Nature. 2002;419(6904):271-277.
- [73] Hutchings J, Stancheva VG, Brown NR, et al. Structure of the complete, membrane-assembled COPII coat reveals a complex interaction network. Nat Commun. 2021;12(1):2034. doi: 10. 1038/s41467-021-22110-6
- [74] Evans R, O'Neill M, Pritzel A, et al. Protein complex prediction with AlphaFold-Multimer. bioRxiv. 2022;2021.10.04.463034. doi: 10.1101/2021.10.04.463034
- [75] Lehmann S, Gumy C, Blatter E, et al. In planta function of compatible solute transporters of the AtProT family. J Exp Bot. 2011;62(2):787-796. doi: 10.1093/jxb/erg320
- [76] Pommerrenig B, Popko J, Heilmann M, et al. SUCROSE TRANSPORTER 5 supplies Arabidopsis embryos with biotin and affects triacylglycerol accumulation. Plant J. 2013;73 (3):392-404. doi: 10.1111/tpj.12037
- [77] Kang J, Hwang JU, Lee M, et al. Pdr-type ABC transporter mediates cellular uptake of the phytohormone abscisic acid. Proc Natl Acad Sci USA. 2010;107(5):2355-2360. doi: 10.1073/pnas.0909222107
- [78] Li B, Zeng Y, Cao W, et al. A distinct giant coat protein complex II vesicle population in Arabidopsis thaliana. Nat Plants. 2021;7 (10):1335-1346. doi: 10.1038/s41477-021-00997-9
- [79] Zheng H, Kunst L, Hawes C, et al. A gfp-based assay reveals a role for RHD3 in transport between the endoplasmic reticulum and Golgi apparatus. Plant J. 2004;37(3):398-414. doi: 10.1046/j.1365-313X.2003.01969.x
- [80] Liu Y, Xiong Y, Bassham DC. Autophagy is required for tolerance of drought and salt stress in plants. Autophagy. 2009;5 (7):954-963. doi: 10.4161/auto.5.7.9290
- [81] Wan C, Ling Q. Functions of autophagy in chloroplast protein degradation and homeostasis. Front Plant Sci. 2022;13:993215. doi: 10.3389/fpls.2022.993215
- [82] Yang Y, Guo Y. Elucidating the molecular mechanisms mediating plant salt-stress responses. New Phytol. 2018;217(2):523-539. doi: 10.1111/nph.14920
- [83] Wu H, Shabala L, Zhou M, et al. Root vacuolar Na(+) sequestration but not exclusion from uptake correlates with barley salt tolerance. Plant J. 2019;100(1):55-67.
- [84] Gong Q, Li P, Ma S, et al. Salinity stress adaptation competence in the extremophile thellungiella halophila in comparison with its relative Arabidopsis thaliana. Plant J. 2005;44(5):826-839. doi: 10. 1111/j.1365-313X.2005.02587.x
- [85] Jang W, Puchkov D, Samso P, et al. Endosomal lipid signaling reshapes the endoplasmic reticulum to control mitochondrial function. Science. 2022;378(6625):eabq5209. doi: 10.1126/science.abq5209
- Axe EL, Walker SA, Manifava M, et al. Autophagosome formation from membrane compartments enriched in phosphatidylinositol 3-phosphate and dynamically connected to the endoplasmic reticulum. J Cell Biol. 2008;182(4):685-701. doi: 10.1083/jcb. 200803137
- [87] Zhuang X, Wang H, Lam SK, et al. A bar-domain protein SH3P2, which binds to phosphatidylinositol 3-phosphate and ATG8, regulates autophagosome formation in arabidopsis. Plant Cell. 2013;25(11):4596-4615. doi: 10.1105/tpc.113.118307
- [88] Ye H, Gao J, Liang Z, et al. Arabidopsis ORP2A mediates er-autophagosomal membrane contact sites and regulates PI3P in plant autophagy. Proc Natl Acad Sci USA. 2022;119(43): e2205314119.
- [89] Chung T, Phillips AR, Vierstra RD. ATG8 lipidation and ATG8-mediated autophagy in Arabidopsis require ATG12 expressed from the differentially controlled ATG12A and ATG12B loci. Plant J. 2010;62(3):483-493. doi: 10.1111/j.1365-313X.2010.04166.x
- [90] Liu R, Zhang R, Yang Y, et al. Monitoring autophagy in rice with GFP-ATG8 marker lines. Front Plant Sci. 2022;13:866367. doi: 10. 3389/fpls.2022.866367
- [91] Clough SJ, Bent AF. Floral dip: a simplified method for agrobacterium-mediated transformation of Arabidopsis thaliana. Plant J. 1998;16(6):735-743. doi: 10.1046/j.1365-313x.1998.00343.x



- [92] Liu Y, Schiff M, Czymmek K, et al. Autophagy regulates programmed cell death during the plant innate immune response. Cell. 2005;121(4):567-577. doi: 10.1016/j.cell.2005.03.007
- [93] Wang D, Weaver ND, Kesarwani M, et al. Induction of protein secretory pathway is required for systemic acquired resistance. Science. 2005;308(5724):1036-1040. doi: 10.1126/science.1108791
- [94] Shimada T, Fuji K, Tamura K, et al. Vacuolar sorting receptor for seed storage proteins in Arabidopsis thaliana. Proc Natl Acad Sci U S A. 2003;100(26):16095-16100. doi: 10.1073/pnas.2530568100
- [95] Jumper J, Evans R, Pritzel A, et al. Highly accurate protein structure prediction with AlphaFold. Nature. (7873):583-589. doi: 10.1038/s41586-021-03819-2
- [96] Drake ZC, Seffernick JT, Lindert S. Protein complex prediction using Rosetta, AlphaFold, and mass spectrometry covalent labeling. Nat Commun. 2022;13(1):7846. doi: 10.1038/s41467-022-35593-8
- [97] Wang C, Schueler-Furman O, Baker D. Improved side-chain modeling for protein-protein docking. Protein Sci. 2005;14 (5):1328-1339.
- [98] Wang C, Bradley P, Baker D. Protein-protein docking with backbone flexibility. J Mol Biol. 2007;373(2):503-519.
- [99] Conway P, Tyka MD, DiMaio F, et al. Relaxation of backbone bond geometry improves protein energy landscape modeling. Protein Sci. 2014;23(1):47-55. doi: 10.1002/pro.2389

- [100] Tyka MD, Keedy DA, Andre I, et al. Alternate states of proteins revealed by detailed energy landscape mapping. J Mol Biol. 2011;405(2):607-618. doi: 10.1016/j.jmb.2010.11.008
- [101] Alford RF, Leaver-Fay A, Jeliazkov JR, et al. The rosetta all-atom energy function for macromolecular modeling and design. J Chem Theory Comput. 2017;13(6):3031-3048. doi: 10.1021/acs.jctc.7b00125
- Conlan B, Stoll T, Gorman JJ, et al. Development of a rapid in planta BioID system as a probe for plasma membrane-associated immunity proteins. Front Plant Sci. 2018;9:1882. doi: 10.3389/fpls. 2018.01882
- [103] Zhang Y, Li Y, Yang X, et al. TurboID-based proximity labeling for in planta identification of protein-protein interaction networks. J Vis Exp. 2020;17(159). doi: 10.3791/60728
- [104] Zhou Y, Zhou B, Pache L, et al. Metascape provides a biologist-oriented resource for the analysis of systems-level datasets. Nat Commun. 2019;10(1):1523. doi: 10.1038/s41467-019-09234-6
- [105] Bindea G, Mlecnik B, Hackl H, et al. ClueGO: a Cytoscape plug-in to decipher functionally grouped gene ontology and pathway annotation networks. Bioinformatics. 2009;25(8):1091-1093. doi: 10.1093/bioinformatics/btp101
- [106] Ni Z, Kim ED, Ha M, et al. Altered circadian rhythms regulate growth vigour in hybrids and allopolyploids. Nature. 2009;457 (7227):327-331. doi: 10.1038/nature07523